



Metallothionein 3-Zinc Axis Suppresses Caspase-11 Inflammasome Activation and Impairs Antibacterial Immunity

OPEN ACCESS

Edited by:

Maciej Lech,
LMU Munich University Hospital,
Germany

Reviewed by:

Amal O. Amer,
The Ohio State University,
United States
Djalma Souza Lima-Junior,
National Institutes of Health (NIH),
United States

*Correspondence:

Kavitha Subramanian Vignesh
Kavitha.Subramanian@uc.edu

Specialty section:

This article was submitted to
Molecular Innate Immunity,
a section of the journal
Frontiers in Immunology

Received: 09 August 2021

Accepted: 15 October 2021

Published: 12 November 2021

Citation:

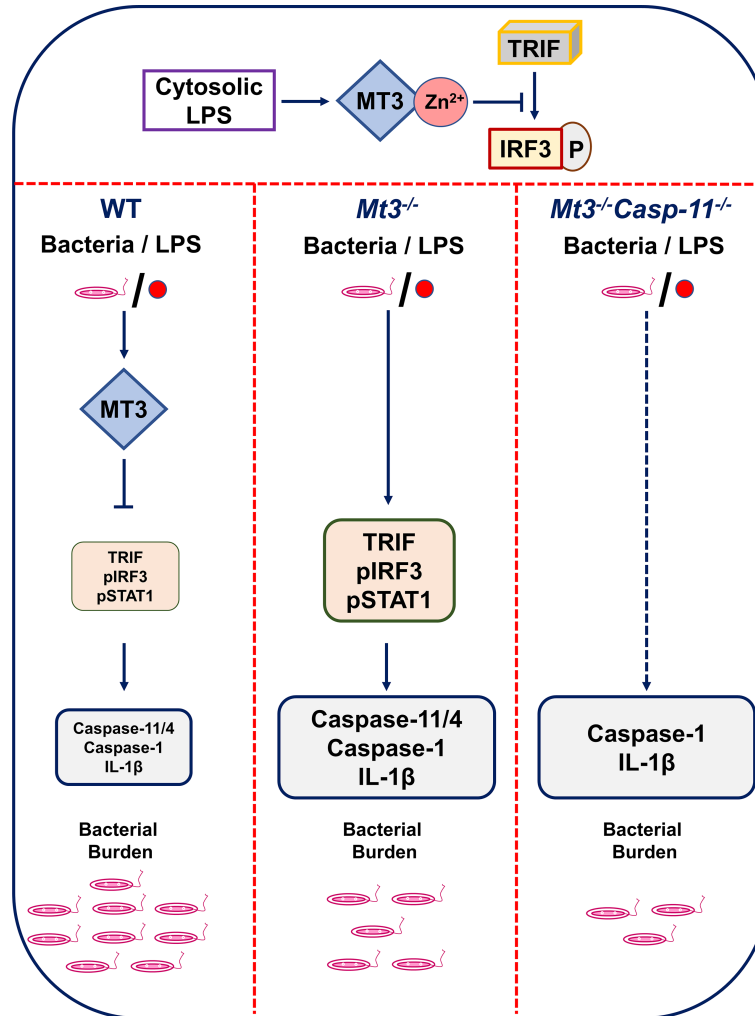
Chowdhury D, Gardner JC, Satpati A,
Nookala S, Mukundan S, Porollo A,
Landro Figueroa JA and
Subramanian Vignesh K (2021)
Metallothionein 3-Zinc Axis
Suppresses Caspase-11
Inflammasome Activation and Impairs
Antibacterial Immunity.
Front. Immunol. 12:755961.
doi: 10.3389/fimmu.2021.755961

Debabrata Chowdhury¹, Jason C. Gardner², Abhijit Satpati³, Suba Nookala³,
Santhosh Mukundan³, Aleksey Porollo^{4,5,6}, Julio A. Landero Figueroa⁷
and Kavitha Subramanian Vignesh^{1*}

¹ Division of Infectious Diseases, College of Medicine, University of Cincinnati, Cincinnati, OH, United States, ² Department of Internal Medicine, Division of Pulmonary, Critical Care, and Sleep Medicine, University of Cincinnati College of Medicine, Cincinnati, OH, United States, ³ Department of Biomedical Sciences, School of Medicine and Health Sciences, University of North Dakota, Grand Forks, ND, United States, ⁴ Center for Autoimmune Genomics and Etiology, Cincinnati Children's Hospital Medical Center, Cincinnati, OH, United States, ⁵ Division of Biomedical Informatics, Cincinnati Children's Hospital Medical Center, Cincinnati, OH, United States, ⁶ Department of Pediatrics, University of Cincinnati, Cincinnati, OH, United States, ⁷ University of Cincinnati/Agilent Technologies Metallomics Center of the Americas, Department of Chemistry, University of Cincinnati, Cincinnati, OH, United States

Non-canonical inflammasome activation by mouse caspase-11 (or human CASPASE-4/5) is crucial for the clearance of certain gram-negative bacterial infections, but can lead to severe inflammatory damage. Factors that promote non-canonical inflammasome activation are well recognized, but less is known about the mechanisms underlying its negative regulation. Herein, we identify that the caspase-11 inflammasome in mouse and human macrophages (M ϕ) is negatively controlled by the zinc (Zn²⁺) regulating protein, metallothionein 3 (MT3). Upon challenge with intracellular lipopolysaccharide (iLPS), M ϕ increased MT3 expression that curtailed the activation of caspase-11 and its downstream targets caspase-1 and interleukin (IL)-1 β . Mechanistically, MT3 increased intramacrophage Zn²⁺ to downmodulate the TRIF-IRF3-STAT1 axis that is prerequisite for caspase-11 effector function. *In vivo*, MT3 suppressed activation of the caspase-11 inflammasome, while caspase-11 and MT3 synergized in impairing antibacterial immunity. The present study identifies an important yin-yang relationship between the non-canonical inflammasome and MT3 in controlling inflammation and immunity to gram-negative bacteria.

Keywords: macrophage, non-canonical inflammasome, zinc, metallothionein, innate immunity, caspase-11 non-canonical inflammasome, MT3



GRAPHICAL ABSTRACT | The MT3-Zn²⁺ axis suppresses TRIF signaling resulting in decreased IRF3 phosphorylation. When MT3 is absent, TRIF-IRF3-STAT1 signaling and non-canonical inflammasome activation are exaggerated. A lack of MT3 augments immunity to gram-negative bacteria, an effect, that is further enhanced by the combined absence of MT3 and caspase-11 *in vivo*. Thus, while MT3 curtails caspase-11 activation, the two molecules act together in compromising antibacterial immunity.

INTRODUCTION

Gram-negative bacteria that cause more than 30% of the total healthcare-associated infections worldwide remain a global concern of morbidity and mortality (1). Assembly of inflammasome complexes during bacterial pathogenesis drives robust inflammation and shapes antibacterial immune responses. The non-canonical inflammasome is activated when innate immune cells such as Mφ sense bacterial ligands in the cytosol (2). LPS from bacterial cell walls enters the cytosol during bacterial escape from vacuoles or *via* rupture of outer membrane vesicles (OMV) (3). iLPS directly binds caspase-11, triggering the non-canonical inflammasome cascade, followed by activation of pro-caspase-1 to caspase-1, processing of pro-IL-1β to mature IL-1β and pyroptosis, a lytic form of programmed cell death. Activation of gasdermin D (GSDMD) by caspase-11 and caspase-1, leads to pore

formation on the cell membrane facilitating the exit of IL-1β from Mφ (4). Unrestricted activation of this inflammatory cascade is a major underlying cause of tissue damage and sepsis-associated mortality (2). Thus, it is crucial to thoroughly understand the molecular cues that guard against excessive activation of the caspase-11 inflammasome. Although factors that promote non-canonical inflammasome activation have been extensively studied, less is known about the mechanisms that negatively regulate it.

MTs are Zn²⁺ regulating proteins induced by endogenous and exogenous stimuli including cytokines, infection, oxidative stress and heavy metals (5, 6). Intracellular availability of total Zn²⁺, exchangeable Zn²⁺ and Zn²⁺ redistribution among proteins is tightly regulated by MTs (7). Mice have 4 MT isoforms (MT1-4), whereas more than 16 MT isoforms are present in humans (8). Our knowledge on the role of the MT family in immune responses largely emerges from studies on MT1 and MT2. We

and others have shown that MT1 and MT2 promote antifungal and antibacterial immunity in M ϕ primarily *via* Zn²⁺ sequestration (9, 10). MT3, on the other hand, suppresses manifestation of proinflammatory phenotypic and metabolic changes and impairs antifungal immunity *in vitro* in M ϕ and *in vivo*. M ϕ expression of MT3 is inducible by IL-4 stimulation. In these cells, MT3 increases intracellular free-Zn²⁺, promotes Zn²⁺ uptake by a prototypic intracellular pathogen and favors microbial survival (11). Thus, MTs and their ability to regulate Zn²⁺ homeostasis intricately ties M ϕ inflammatory responses to antimicrobial defense.

Zn²⁺ is indispensable in many biochemical processes due to its role in structural and catalytic functions of enzymes and macromolecules. Zn²⁺ excess or deficiency compromises the development and function of immune cells including monocytes and M ϕ , leading to increased risk of infection (12). Zn²⁺ also has a profound role as a signaling ion attributable to the transient changes in intracellular exchangeable Zn²⁺. LPS triggers increased Zn²⁺ import in leukocytes, monocytes and M ϕ (13, 14). In peripheral blood mononuclear cells (PBMCs) and human M ϕ (hM ϕ), LPS-induced Zn²⁺ influx promotes IL-1 β production (14). In contrast, exogenous exposure to Zn²⁺ in human monocytes may reduce IL-1 β production due to inhibition of nucleotide phosphodiesterases (15). Thus, the effects of Zn²⁺ on signaling and cytokine production are context and Zn²⁺ concentration-dependent. Changes in ion flux, specifically K⁺ and Cl⁻ egress and intracellular mobilization of Ca²⁺ underlie canonical nod-like receptor pyrin domain containing-3 (NLRP3) inflammasome activation (16). Intriguingly, Zn²⁺ exerts disparate effects on activation of this cascade. Long-term Zn²⁺ depletion disrupts lysosomal integrity leading to increased activation of the canonical NLRP3 inflammasome (17). On the other hand, short-term chelation of Zn²⁺ attenuates the canonical pathway due to impaired function of the pannexin-1 receptor (18).

The importance of Zn²⁺ regulation by MTs in the non-canonical inflammasome pathway remain unexplored. Given the suppressive role of MT3 in M ϕ inflammatory responses (19), we hypothesized that MT3 negatively regulates the highly inflammatory caspase-11 activation cascade. Bioinformatics analysis predicted the involvement of MT3 in regulating non-canonical inflammasome-associated pathways. Using a combination of protein-protein interaction network analysis, immunological and mass-spectrometric approaches, we demonstrate that triggering caspase-11 activation results in a profound, gradual increase in the M ϕ Zn²⁺ pool mediated by MT3. The increase in Zn²⁺ attenuates signaling *via* toll/interleukin-1 receptor (TIR) domain containing adaptor-inducing interferon (IFN) β - interferon regulatory factor 3 - signal transducer and activator of transcription factor 1 (TRIF-IRF3-STAT1), a pathway that is prerequisite for caspase-11 inflammasome activation (20). Zn²⁺ deficiency augments, whereas Zn²⁺ supplementation suppresses the non-canonical inflammasome in M ϕ . Using whole-body *Mt3*^{-/-} and myeloid-MT3-deficient mice, we elucidate that MT3 blunts non-canonical inflammasome activation *in vitro* and *in vivo* upon challenge with iLPS or gram-negative bacteria but not gram-positive bacteria. Importantly, this function of MT3 is conserved

in hM ϕ . Although caspase-11 and MT3 form a negative regulatory loop, we find that these two molecules synergize in compromising antibacterial immunity. Our data uncover a previously unknown yin-yang relationship whereby the MT3-Zn²⁺ axis exerts a brake on non-canonical inflammasome activation but the functions of MT3 and caspase-11 converge in crippling immunity to invading bacteria (see **Graphical Abstract**).

RESULTS

MT3 Suppresses Activation of the Non-Canonical Inflammasome *In Vitro*

MT3 attenuates cell death in neuronal and glial cells, but the precise underlying mechanisms are not fully understood (21). As non-canonical inflammasome activation leads to pyroptotic cell death, we investigated if MT3 effector function is related to caspase-11 activation in M ϕ . We explored whether MT3 is involved in inflammatory and cell-death processes using functional enrichment analysis. We assessed protein-protein interaction networks of MT3 in *Mus musculus* and *Homo sapiens* using the STRING database (22). The MT3 interaction partners significantly enriched 15 mouse and 43 human gene ontology categories for biological processes (GO BP) related to programmed cell death (PCD), LPS responses, signaling *via* TRIF, IL-1 and type-I IFN, cytokine responses and several immune processes. A complete network of MT3 interactions and GO BP categories is in **Table 1, Supplementary Table S1, Supplementary Files S1 and S2**. PCD and LPS responses are linked to inflammasome activation and more specifically, TRIF and type-I IFN signaling are tied to the non-canonical inflammasome pathway. A lack of TRIF signaling ablates non-canonical inflammasome activation in response to iLPS without impacting M ϕ response to canonical NLRP3 triggers such as ATP and nigericin (20). Thus, our bioinformatics analysis together with our previously reported role for MT3 in suppressing proinflammatory responses in M ϕ led us to investigate whether MT3 negatively regulates the non-canonical inflammasome pathway.

In M ϕ , exposure to iLPS triggers caspase-11 activation and cell death by pyroptosis (2). We directly assessed if MT3 regulates non-canonical inflammasome activation using WT and *Mt3*^{-/-} mice. BMDM ϕ were exposed to iLPS or vehicle control and time-dependent changes in the gene expression of *Mt1*, *Mt2* and *Mt3* were examined. *Mt3* expression increased gradually from 1 hour (h) and peaked at 48h in WT BMDM ϕ challenged with iLPS (**Figure 1A**). The expression of *Mt1* and *Mt2* peaked at 6h, but receded over time in both WT and *Mt3*^{-/-} BMDM ϕ (**Supplementary Figures S1A, B**). To determine whether exogenous LPS had an effect on MT3, we stimulated WT BMDM ϕ with extracellular LPS (exLPS) for 48h. While iLPS increased *Mt3* expression by 10-fold, the fold increase observed with exLPS challenge was much lower (**Figure 1B**).

Next, we examined if MT3 regulated non-canonical inflammasome activation by assessing pro- and active forms of caspase-11, caspase-1 and IL-1 β in cell lysates and supernatants

TABLE 1 | See also **Supplementary Table S1** and **Files S1, S2** | Protein interaction network of *Mus musculus* MT3 to determine functionally enriched GO BP categories using the STRING database.**Protein-Protein Interaction Network of *Homo sapiens* MT3**

Sl. No	Term ID	Term Description	FDR	Protein Labels
1	GO:0060548	Negative regulation of cell death	2.30E-10	NGFR,MT3,RIPK2,CAT,TRAF2,RIPK1,SLC40A1,SOD1,RPS27A,EGFR,APP,ALB,SNCB,FAIM2,ERBB4,GPX4,SLC30A10,TXN,MAG,UBA52,GPX1,TRAF6,UBC,SOD2,AKT1,IKBK
2	GO:0043069	Negative regulation of programmed cell death	6.51E-09	NGFR,MT3,RIPK2,CAT,TRAF2,RIPK1,SLC40A1,SOD1,RPS27A,EGFR,ALB,SNCB,FAIM2,ERBB4,GPX4,SLC30A10,MAG,UBA52,GPX1,TRAF6,UBC,SOD2,AKT1
3	GO:0043066	Negative regulation of apoptotic process	2.32E-08	NGFR,MT3,RIPK2,CAT,TRAF2,RIPK1,SLC40A1,SOD1,RPS27A,EGFR,ALB,SNCB,FAIM2,ERBB4,SLC30A10,MAG,UBA52,GPX1,TRAF6,UBC,SOD2,AKT1
4	GO:0010941	Regulation of cell death	2.59E-08	TNFRSF1A,NGFR,MT3,RIPK2,CAT,TRAF2,RIPK1,SLC40A1,SOD1,RPS27A,EGFR,APP,ALB,SNCB,FAIM2,RTN4,ERBB4,GPX4,SLC30A10,TXN,MAG,FOXO3,UBA52,CYLD,GPX1,TRAF6,UBC,SOD2,AKT1,IKBK
5	GO:0043067	Regulation of programmed cell death	8.35E-08	TNFRSF1A,NGFR,MT3,RIPK2,CAT,TRAF2,RIPK1,SLC40A1,SOD1,RPS27A,EGFR,APP,ALB,SNCB,FAIM2,RTN4,ERBB4,GPX4,SLC30A10,MAG,FOXO3,UBA52,CYLD,GPX1,TRAF6,UBC,SOD2,AKT1
6	GO:0042981	Regulation of apoptotic process	2.74E-07	TNFRSF1A,NGFR,MT3,RIPK2,CAT,TRAF2,RIPK1,SLC40A1,SOD1,RPS27A,EGFR,APP,ALB,SNCB,FAIM2,RTN4,ERBB4,SLC30A10,MAG,FOXO3,UBA52,CYLD,GPX1,TRAF6,UBC,SOD2,AKT1
7	GO:0010942	Positive regulation of cell death	1.84E-06	TNFRSF1A,NGFR,MT3,RIPK2,TRAF2,RIPK1,SOD1,RPS27A,APP,ERBB4,FOXO3,UBA52,CYLD,TRAF6,UBC,SOD2,AKT1
8	GO:0035666	TRIF-dependent toll-like receptor signaling pathway	8.19E-06	RIPK1,RPS27A,UBA52,UBC,IKBK
9	GO:0070498	Interleukin-1-mediated signaling pathway	1.00E-05	RIPK2,RPS27A,UBA52,TRAF6,UBC,IKBK
10	GO:0045089	Positive regulation of innate immune response	2.38E-05	RIPK2,EREG,RIPK1,RPS27A,DDX58,UBA52,CYLD,TRAF6,UBC,IKBK
11	GO:0071345	Cellular response to cytokine stimulus	3.60E-05	RTN4R,TNFRSF1A,NGFR,MT3,RIPK2,EREG,TRAF2,RIPK1,SOD1,RPS27A,AQP4,FOXO3,UBA52,TRAF6,UBC,SOD2,AKT1,IKBK
12	GO:1903209	Positive regulation of oxidative stress-induced cell death	4.97E-05	RIPK1,SOD1,APP,FOXO3
13	GO:0045088	Regulation of innate immune response	5.35E-05	RIPK2,EREG,RIPK1,RPS27A,APP,DDX58,UBA52,CYLD,TRAF6,UBC,IKBK
14	GO:0002757	Immune response-activating signal transduction	0.00015	RIPK2,RIPK1,RPS27A,RNF31,DDX58,UBA52,CYLD,TRAF6,UBC,IKBK
15	GO:0002684	Positive regulation of immune system process	0.00017	RIPK2,EREG,TRAF2,RIPK1,RPS27A,APP,RNF31,RBP4,DDX58,FOXO3,UBA52,CYLD,TRAF6,UBC,AKT1,IKBK
16	GO:0001959	Regulation of cytokine-mediated signaling pathway	0.00022	TNFRSF1A,RIPK2,TRAF2,RIPK1,RNF31,CYLD,IKBK
17	GO:0006915	apoptotic process	0.00025	TNFRSF1A,NGFR,MT3,RIPK2,TRAF2,RIPK1,APP,FAIM2,RTN4,ERBB4,FOXO3,GPX1,SOD2,AKT1,GNB1,IKBK
18	GO:0012501	Programmed cell death	0.00031	TNFRSF1A,NGFR,MT3,RIPK2,TRAF2,RIPK1,APP,FAIM2,RTN4,ERBB4,FOXO3,CYLD,GPX1,SOD2,AKT1,GNB1,IKBK
19	GO:1902175	Regulation of oxidative stress-induced intrinsic apoptotic signaling pathway	0.00032	SOD1,GPX1,SOD2,AKT1
20	GO:1902042	Negative regulation of extrinsic apoptotic signaling pathway <i>via</i> death domain receptors	0.00056	TRAF2,RIPK1,FAIM2,GPX1
21	GO:0050778	Positive regulation of immune response	0.00064	RIPK2,EREG,TRAF2,RIPK1,RPS27A,RNF31,DDX58,UBA52,CYLD,TRAF6,UBC,IKBK
22	GO:1903202	Negative regulation of oxidative stress-induced cell death	0.0011	TXN,GPX1,SOD2,AKT1
23	GO:2001236	Regulation of extrinsic apoptotic signaling pathway	0.0018	TRAF2,RIPK1,FAIM2,CYLD,GPX1,AKT1
24	GO:0002376	Immune system process	0.0029	TNFRSF1A,NGFR,RIPK2,TTR,CAT,NTS,HNF1A,RIPK1,SLC40A1,PRDX1,SOD1,RPS27A,APP,RNF31,ATP7A,DDX58,AQP4,MAG,UBA52,CYLD,SERPINA1,TRAF6,UBC,AKT1,IKBK
25	GO:0097300	Programmed necrotic cell death	0.0034	TRAF2,RIPK1,CYLD
26	GO:0071356	Cellular response to tumor necrosis factor	0.0045	TNFRSF1A,NGFR,TRAF2,RIPK1,FOXO3,AKT1
27	GO:0032743	Positive regulation of interleukin-2 production	0.0046	RIPK2,TRAF2,TRAF6
28	GO:0032755	Positive regulation of interleukin-6 production	0.0049	RIPK2,EREG,DDX58,TRAF6
29	GO:0010940	Positive regulation of necrotic cell death	0.0062	MT3,RIPK1
30	GO:0097190	Apoptotic signaling pathway	0.0063	TNFRSF1A,NGFR,TRAF2,RIPK1,FOXO3,GPX1,SOD2
31	GO:2001233	Regulation of apoptotic signaling pathway	0.0066	TRAF2,RIPK1,SOD1,FAIM2,CYLD,GPX1,SOD2,AKT1
32	GO:2001234	Negative regulation of apoptotic signaling pathway	0.0068	TRAF2,RIPK1,FAIM2,GPX1,SOD2,AKT1
33	GO:0050852	T cell receptor signaling pathway	0.0096	RIPK2,RNF31,TRAF6,IKBK
34	GO:0097191	Extrinsic apoptotic signaling pathway	0.0096	TNFRSF1A,TRAF2,RIPK1,FOXO3
35	GO:2001242	Regulation of intrinsic apoptotic signaling pathway	0.0096	SOD1,CYLD,GPX1,SOD2,AKT1
36	GO:0070673	Response to interleukin-18	0.01	RIPK2,AKT1

(Continued)

TABLE 1 | Continued

Protein-Protein Interaction Network of <i>Homo sapiens</i> MT3				
Sl. No	Term ID	Term Description	FDR	Protein Labels
37	GO:2001238	Positive regulation of extrinsic apoptotic signaling pathway	0.0145	TRAF2,RIPK1,CYLD
38	GO:0060760	Positive regulation of response to cytokine stimulus	0.0152	RIPK2,TRAF2,DDX58
39	GO:0001819	Positive regulation of cytokine production	0.0215	RIPK2,EREG,TRAF2,RIPK1,SOD1,DDX58,TRAF6
40	GO:0002824	Positive regulation of adaptive immune response based on somatic recombination of immune receptors built from immunoglobulin superfamily domains	0.0476	RIPK2,TRAF2,TRAF6
41	GO:0045639	Positive regulation of myeloid cell differentiation	0.0476	RIPK1,FOXO3,TRAF6
42	GO:0031663	Lipopolysaccharide-mediated signaling pathway	0.0493	RIPK2,AKT1
43	GO:2001235	Positive regulation of apoptotic signaling pathway	0.05	TRAF2,RIPK1,SOD1,CYLD

of WT and *Mt3*^{-/-} BMDM ϕ challenged with iLPS. A lack of MT3 exacerbated activation of caspase-11 in cell lysates, and caspase-1 and IL-1 β in culture supernatants. Pro-caspase-11, pro-caspase-1 and pro-IL-1 β proteins in cell lysates were similar between iLPS treated WT and *Mt3*^{-/-} BMDM ϕ (Figure 1C). We further examined combined lysate and supernatant samples and found increased caspase-11 activation in *Mt3*^{-/-} BMDM ϕ challenged with iLPS (Figure 1D). Thus, the differences observed were not merely a result of reduced release of the active forms from cells, but an increase in non-canonical inflammasome activation in *Mt3*^{-/-} BMDM ϕ . Intracellular transfection of LPS at two different concentrations (2 and 10 μ g/ml) yielded similar results (Figures 1C, D). We then examined the levels of IL-1 α in supernatants of WT and *Mt3*^{-/-} BMDM ϕ challenged with iLPS. In contrast to IL-1 β , IL-1 α was moderately reduced in the supernatants of *Mt3*^{-/-} BMDM ϕ (Supplementary Figures S1C, D). We note that although IL-1 α is activated by caspase-11, it is characteristically different from IL-1 β , as it exists in both membrane-bound and secreted forms that are differentially regulated, and both pro- and cleaved IL-1 α are bioactive (23–25).

MT3 Represses CASPASE-4 Activation and Antibacterial Resistance in Human M ϕ

Gram-negative bacteria activate the non-canonical inflammasome via CASPASE-4 in hM ϕ (26). We investigated whether human MT3, similar to mouse MT3, suppressed non-canonical inflammasome activation and antibacterial immunity. Human monocyte-derived M ϕ obtained from PBMCs were transfected with scramble siRNA or MT3 siRNA followed by transfection with iLPS. To assess siRNA specificity, we analyzed the expression of MT3 and MT2A genes. MT3, but not MT2A expression was silenced in MT3 siRNA transfected hM ϕ (Figure 2A). MT3 deficiency resulted in elevated activation of CASPASE-4 and heightened release of IL-1 β from hM ϕ (Figures 2B, C). We previously showed that a lack of MT3 increased resistance of mouse BMDM ϕ to *Escherichia coli* (19). We therefore queried whether silencing MT3 in hM ϕ impaired bacterial clearance *in vitro*. hM ϕ treated with scramble siRNA or MT3 siRNA were infected with *E. coli* K12 for 24h. MT3-deficient hM ϕ exerted a sharp decline in intracellular bacterial survival compared to control hM ϕ (Figure 2D).

MT3 Dampens Antibacterial Resistance and Caspase-11 Inflammasome Activation *In Vitro* and *In Vivo*

We examined whether MT3 regulated antibacterial immunity and non-canonical inflammasome activation *in vitro* and *in vivo*. WT and *Mt3*^{-/-} BMDM ϕ were infected with *E. coli*. After 24h, bacterial survival was reduced in *Mt3*^{-/-} BMDM ϕ (Figure 2E). Next, we infected WT and *Mt3*^{-/-} mice *in vivo* intraperitoneally (*i.p.*) with *E. coli* for 6h. Compared to WT mice, MT3 deficiency bolstered bacterial elimination from the blood and moderately improved bacterial clearance in the kidney and peritoneal lavage (Figure 2F). Caspase-11, GSDMD (N-terminal) and caspase-1 activation were heightened in kidney homogenates of infected *Mt3*^{-/-} mice compared to infected WT mice (Figure 2G). The decrease in pro-GSDMD of *Mt3*^{-/-} mice may be explained by increased conversion of pro- to active-GSDMD form (Figure 2G). IL-1 β in the peritoneal lavage was significantly elevated ($p < 0.01$) and serum IL-1 β exhibited a trend towards increase in infected *Mt3*^{-/-} mice compared to WT controls (Figure 2H). To determine if this response is consistent upon LPS challenge *in vivo*, we primed mice *i.p.* with poly(I:C) for 6h and challenged them *i.p.* with ultrapure LPS. After 18h, IL-1 β was elevated in the peritoneal lavage and serum of *Mt3*^{-/-} mice compared to WT mice (Figure 2I). We further queried the impact of MT3 on LPS-induced sepsis. WT and *Mt3*^{-/-} mice were challenged with ultrapure LPS (20 mg/kg) and assayed for weight loss, murine sepsis scores (MSS) as reported previously (27) and survival. MT3 deficiency resulted in greater weight loss and increased sepsis scores, but both genotypes similarly succumbed to septic shock (Supplementary Figures S2A-C).

We then investigated whether MT3 increased susceptibility to other gram-negative bacteria. WT and *Mt3*^{-/-} mice were infected intranasally (*i.n.*) with a virulent, heavily encapsulated strain of *Klebsiella pneumoniae* (KP2 2-70). MT3 deficiency significantly ($p < 0.05$) improved *K. pneumoniae* clearance in the spleen, but no changes were observed in the lung and kidney (Figure 2J). Gram-positive bacteria activate caspase-11 via the NLRP6 inflammasome (28). We determined whether the increased non-canonical inflammasome activation and antibacterial resistance observed in *Mt3*^{-/-} mice extended to gram-positive bacterial infection. WT and *Mt3*^{-/-} mice were challenged subcutaneously (*s.q.*) with a clinical

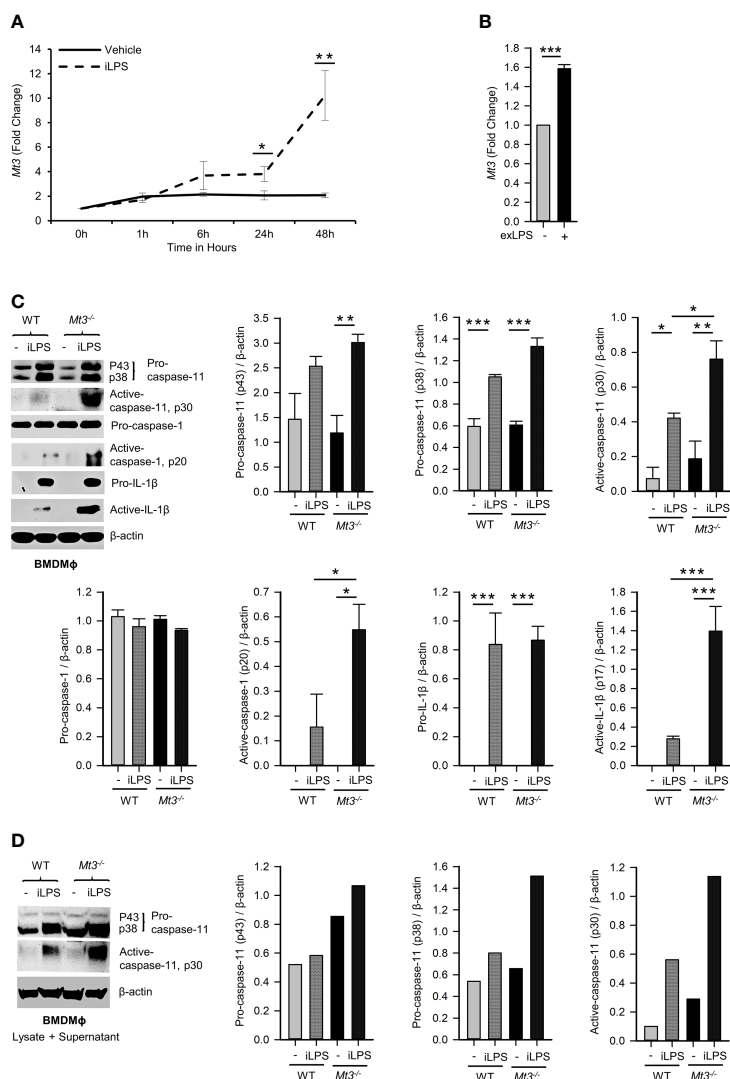


FIGURE 1 | See also **Supplementary Figure S1** MT3 suppresses caspase-11 inflammasome activation in BMDM ϕ . qRT-PCR analysis of *Mt3* expression in WT BMDM ϕ stimulated with **(A)** iLPS (2 μ g/ml) or vehicle control, 3-5 independent experiments and **(B)** exLPS (10 μ g/ml) for 48h, 3 independent experiments, two-tailed t-test. **(C)** Western Blots of pro- and active-caspase-11, pro-caspase-1, pro-IL1 β and β -actin in cell lysates and active-caspase-1 and active-IL-1 β in supernatants of WT and *Mt3*^{-/-} BMDM ϕ stimulated with iLPS (10 μ g/ml) or vehicle for 48h. Bar graphs are densitometric analysis of targets normalized to β -actin, 3-4 independent experiments, one-way ANOVA, data are mean \pm SEM. **(D)** Western Blots of pro- and active-caspase-11 and β -actin in lysate + supernatant samples from WT and *Mt3*^{-/-} BMDM ϕ stimulated with iLPS (2 μ g/ml) or vehicle for 48h. Bar graphs are densitometric analysis of targets normalized to β -actin. **p* < 0.05, ***p* < 0.01, ****p* < 0.001.

isolate of Group-A-Streptococcus GAS5448 (29). After 72h, *Mt3*^{-/-} mice manifested significantly (*p*<0.05) reduced GAS burden in the kidney and spleen compared to WT mice. Bacterial CFUs in the blood exhibited a similar trend (**Supplementary Figure S2D**). Importantly, although *Mt3*^{-/-} mice exhibited higher activation of caspase-1 and IL-1 β , the levels of active caspase-11 and pro-caspase-11 were diminished in GAS-infected *Mt3*^{-/-} mice compared to WT mice (**Supplementary Figure S2E**). Thus, although MT3 compromises resistance to both gram-negative and gram-positive bacteria, it specifically suppresses non-canonical inflammasome signaling in response to gram-negative microbial triggers.

Caspase-11 Synergizes With MT3 in Impairing *E. coli* Clearance In Vivo

Caspase-11 is crucial in antibacterial defenses particularly against gram-negative bacteria, although some studies have suggested a detrimental role for caspase-11 in bacterial elimination (30–35). MT3 suppressed antibacterial immunity as well as non-canonical inflammasome activation. Thus, we investigated whether the heightened immunity to *E. coli* in *Mt3*^{-/-} mice was due to increased non-canonical inflammasome activation. We infected WT, *Casp-11*^{-/-}, *Mt3*^{-/-}, and *Mt3*^{-/-}*Casp-11*^{-/-} mice (**Supplementary Figure S3A**) *i.p.* with *E. coli* and assessed bacterial burden 6h post-infection. Compared to WT mice, bacterial elimination was

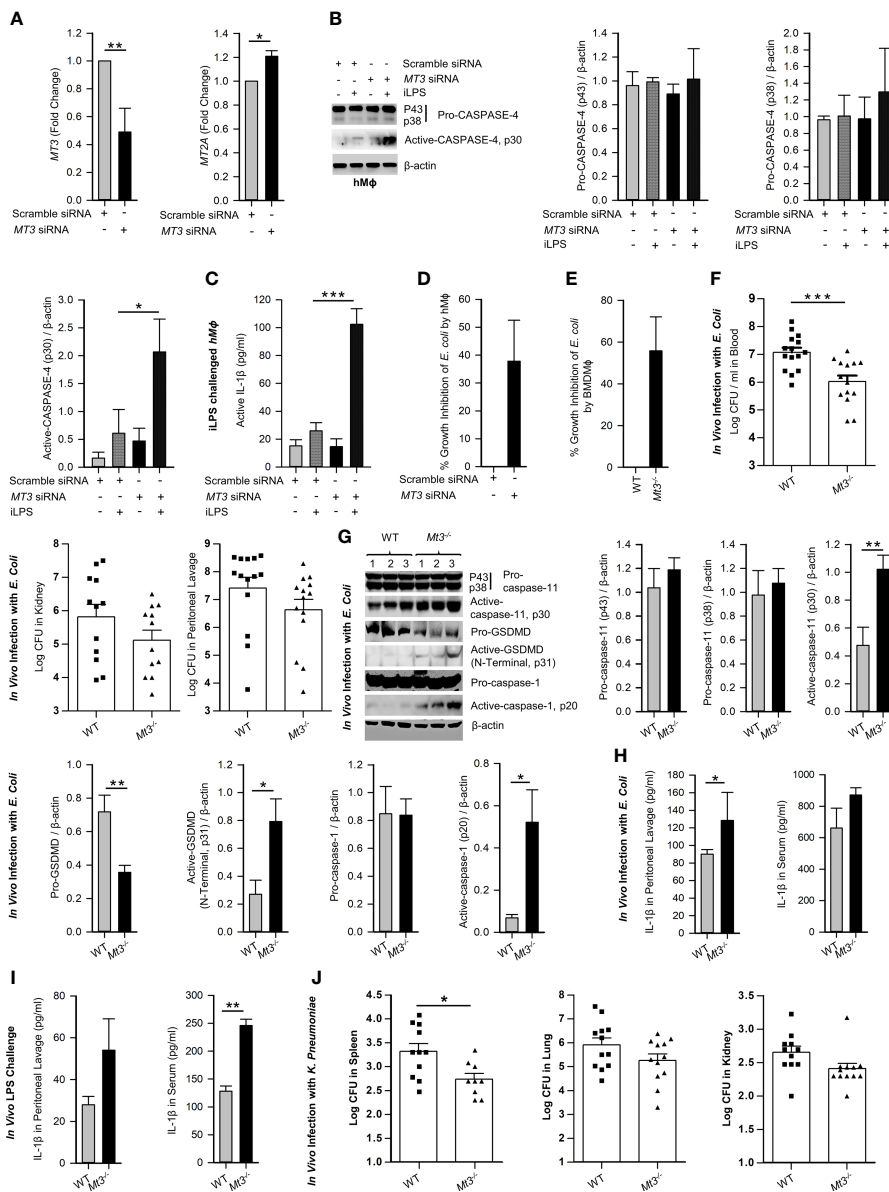


FIGURE 2 | See also **Supplementary Figure S2**. MT3 curtails CASPASE-4 and caspase-11 signaling and antibacterial immunity in hMφ and *in vivo*. **(A)** MT3 and MT2A expression analyzed by qRT-PCR in hMφ transfected with scramble siRNA or MT3 siRNA for 24h, 3 independent experiments, two-tailed t-test. **(B)** Scramble siRNA or MT3 siRNA treated hMφ stimulated with ILPS (10 μg/ml) or vehicle for 48h. Immunoblots of pro-CASPASE-4 and active-CASPASE-4 in cell extracts, 3 independent experiments, one-way ANOVA. **(C)** Active-IL-1β measured by ELISA in supernatants of hMφ treated as above, 3 independent experiments, one-way ANOVA. **(D)** *E. coli* growth inhibition in hMφ transfected with MT3 siRNA and infected with 25 *E. coli* (K12): 1 hMφ for 24h compared to scramble siRNA treated hMφ, 3 independent experiments, two-tailed t-test. **(E)** *E. coli* growth inhibition in WT and *Mt3*^{-/-} BMDMφ infected with 25 *E. coli* (K12):1 hMφ for 24h, 4 independent experiments, two-tailed t-test. **(F)** WT and *Mt3*^{-/-} mice infected *i.p.* with 1X10⁹ *E. coli* for 6h, log CFUs of *E. coli* in blood, kidney and peritoneal lavage samples, n = 12-15 per group, two-tailed t-test. **(G)** Western blots of inflammasome mediators in kidney homogenates of WT and *Mt3*^{-/-} mice infected as above, n = 6 per group, two-tailed t-test. **(H)** WT and *Mt3*^{-/-} mice infected *i.p.* with 1 X10⁹ *E. coli* for 1h and IL-1β measured in peritoneal lavage and serum by ELISA. n = 3 per group, two-tailed t-test. **(I)** WT and *Mt3*^{-/-} mice primed *i.p.* with poly(I:C) (10 mg/kg) for 6h and challenged with LPS (2 mg/kg) *i.p.* After 18h, IL-1β was measured in peritoneal lavage and serum by ELISA, n = 3/group, two-tailed t-test. **(J)** Bacterial growth in spleen, lung and kidney of WT and *Mt3*^{-/-} mice infected *i.n.* with *K. pneumoniae* (4 X10⁴ CFUs/mouse) for 48h, n = 8-12 per group, two-tailed t-test, data are mean ± SEM. *p < 0.05, **p < 0.01, ***p < 0.001.

enhanced in *Mt3*^{-/-} and *Casp-11*^{-/-} mice but this response was further exacerbated in *Mt3*^{-/-} mice lacking caspase-11 (**Figure 3A**). These data indicate that the combined absence of MT3 and caspase-11 improves resistance to gram-negative bacterial

infection. We then analyzed caspase-11 inflammasome mediators in kidney homogenates harvested 6h post-infection. Mice lacking MT3, or caspase-11, exhibited elevated activation of GSDMD (N-terminal), caspase-1 and IL-1β compared to WT mice (**Figure 3B**).

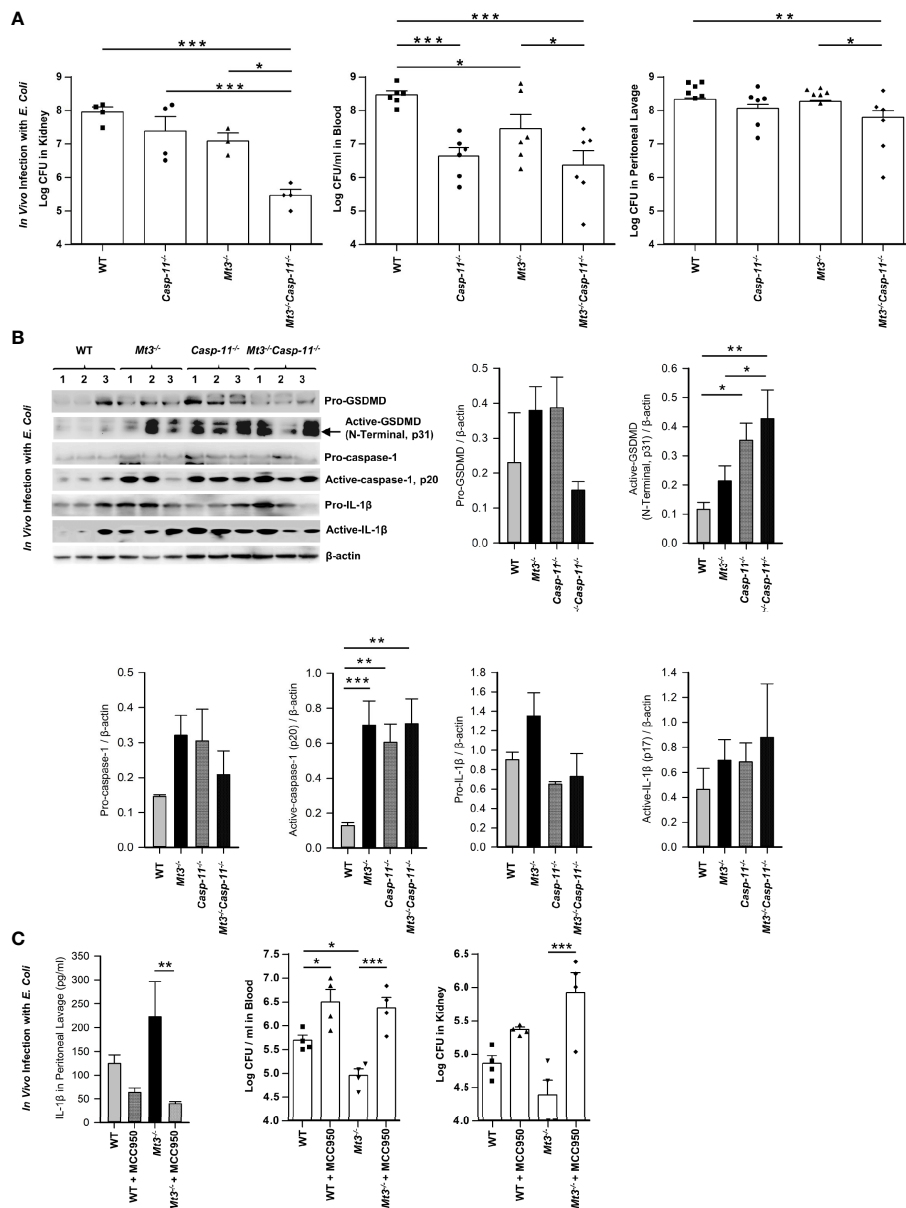


FIGURE 3 | See also **Supplementary Figure S3** Caspase-11 synergizes with MT3 in impairing bacterial clearance. WT, *Casp-11*^{-/-}, *Mt3*^{-/-} and *Casp-11*^{-/-}*Mt3*^{-/-} mice were infected *i.p.* with *E. coli* (1×10^9 CFUs/mouse) for 6h. **(A)** Bacterial CFUs measured in kidney, blood and peritoneal lavage, $n = 3-6$ per group, one-way ANOVA. **(B)** Western blots of pro-GSDMD, active-GSDMD (p31), pro-caspase-1, active-caspase-1, pro-IL1β and active-IL-1β in kidney homogenates, $n = 3-6$ per group, one-way ANOVA, data are mean \pm SEM. **(C)** WT and *Mt3*^{-/-} mice treated *i.p.* with MCC950 (1 mg/mouse) or PBS and infected *i.p.* with *E. coli* (1×10^9 CFUs/mouse) for 6h. IL1β was measured by ELISA in peritoneal lavage, $n = 6$ per group, one-way ANOVA, data are mean \pm SEM. Bacterial CFUs in whole blood and kidney, $n = 4$ per group, one-way ANOVA, data are mean \pm SEM. * $p < 0.05$, ** $p < 0.01$, *** $p < 0.001$.

These changes were also observed in the *Mt3*^{-/-}*Casp-11*^{-/-} mice. Since GSDMD is a target of caspase-11 as well as caspase-1 (36), an elevation in active GSDMD may result from higher caspase-1 activation observed in mice lacking MT3, caspase-11 or both. Caspase-8, a pro-apoptotic caspase, collaborates with caspase-11 to mediate systemic inflammation and septic shock (37, 38). Moreover, caspase-8, in addition to caspase-1 can directly cleave IL-1β. We therefore analyzed caspase-8 in kidney homogenates

from *E. coli* infected WT, *Mt3*^{-/-}, *Casp-11*^{-/-} and *Mt3*^{-/-}*Casp-11*^{-/-} mice. Caspase-11 negatively influenced the activation of caspase-8 (**Supplementary Figure S3B**).

The above data demonstrate that even when caspase-11 is absent, *Mt3*^{-/-} mice exert heightened levels of active caspase-1, active IL-1β and antibacterial immunity. We therefore queried whether improved bacterial elimination in the absence of MT3 was facilitated by the canonical NLRP3 inflammasome. WT and

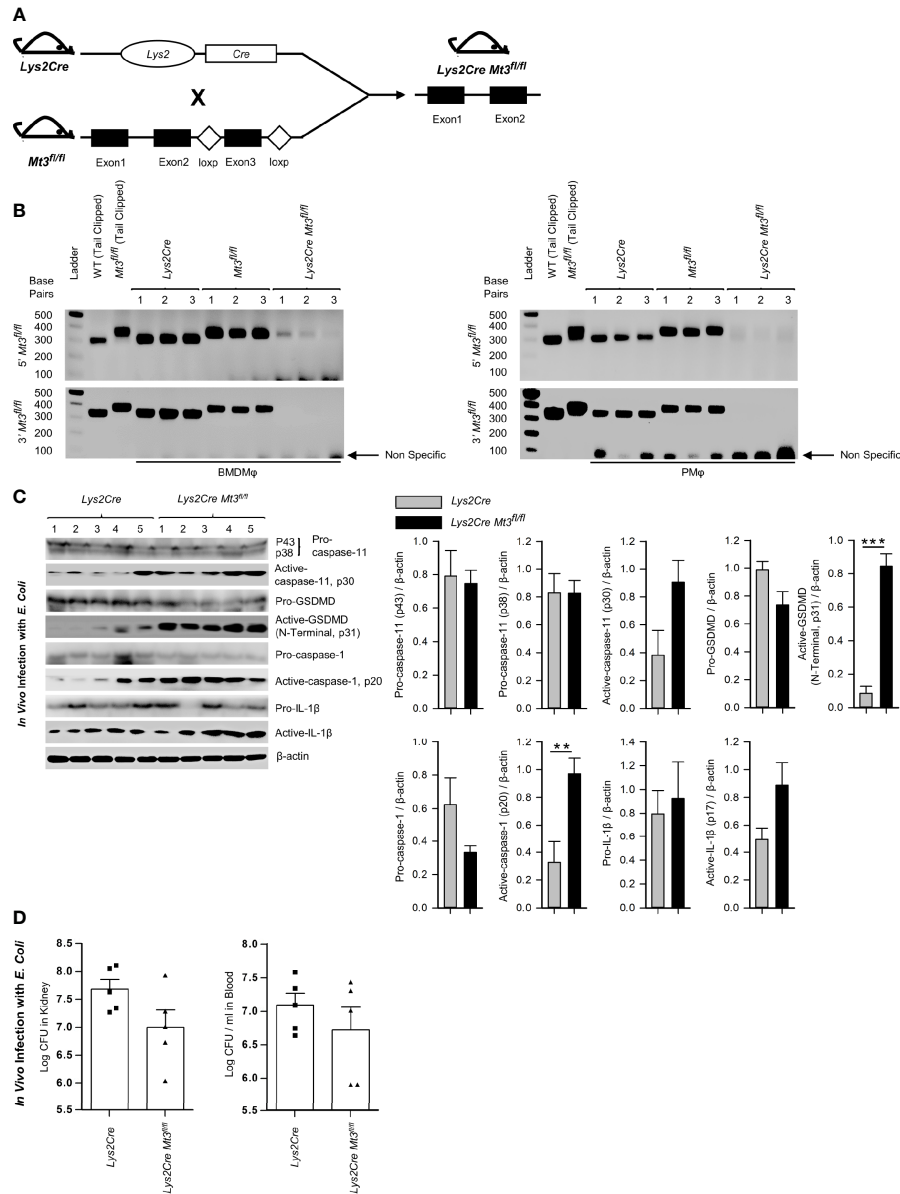


FIGURE 4 | See also **Supplementary Figure S4** Myeloid-MT3 suppresses non-canonical inflammasome activation and blunts gram-negative bacterial clearance *in vivo*. **(A)** Generation of *Mt3^{fl/fl}* mice by inserting loxP sites flanking exon 3 of the *Mt3* gene using the CRISPR-Cas9 gene targeting approach. *Mt3^{fl/fl}* mice crossed with *Lys2Cre* mice to obtain *Lys2Cre Mt3^{fl/fl}* mice. **(B)** Efficacy of myeloid *Mt3* deletion assessed by genotyping peritoneal Mφ (PMφ) and BMDMφ from *Lys2Cre*, *Mt3^{fl/fl}* and *Lys2Cre Mt3^{fl/fl}* mice. Gel electrophoresis analysis demonstrating efficient deletion of the *Mt3* gene from BMDMφ and PMφ of *Lys2Cre Mt3^{fl/fl}* mice. **(C)** Western blots of pro-caspase-11, active-caspase-11, pro-GSDMD, active-GSDMD (p31), pro-caspase-1, active-caspase-1, pro-IL1β and active-IL-1β in whole kidney homogenates of mice infected as above, n = 3-5 per group, two-tailed t-test. **(D)** Bacterial CFUs in kidney and whole blood of *Lys2Cre* and *Lys2Cre Mt3^{fl/fl}* mice infected *i.p.* with *E. coli* (1×10^9 CFUs/mouse) for 6h, n = 3-5 per group, two-tailed t-test, data are mean ± SEM. **p < 0.01, ***p < 0.001.

Mt3^{-/-} mice were treated *i.p.* with MCC950 (NLRP3 inhibitor) followed by infection *i.p.* with *E. coli*. Treatment with MCC950 reduced IL-1β levels and sharply blunted antibacterial resistance in the blood and kidney of *Mt3^{-/-}* mice compared to vehicle-treated controls. Bacterial burdens were also elevated in WT mice by NLRP3 inhibition (**Figure 3C**). Collectively, these data demonstrate that MT3 negatively controls activation of the

non-canonical inflammasome and that both MT3 and caspase-11 cripple resistance to bacterial infection.

Myeloid MT3 Orchestrates Negative Control of the Non-Canonical Inflammasome

To affirm that the effects on caspase-11 inflammasome activation observed in the *Mt3^{-/-}* mice were dependent on myeloid-MT3, we

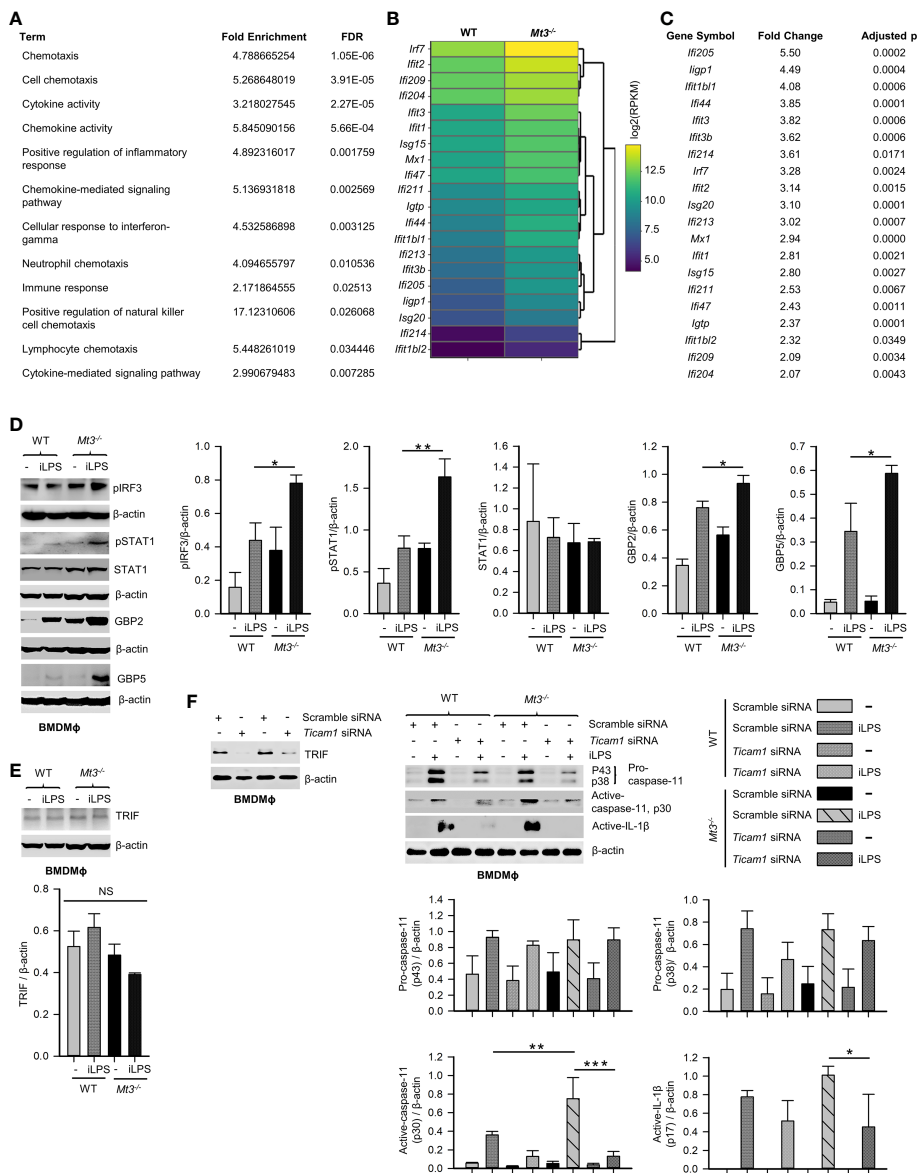


FIGURE 5 | See also **Supplementary Figure S5** MT3 thwarts TRIF-IRF3-STAT1 signaling to suppress non-canonical inflammasome activation. **(A)** Functional enrichment analysis of differentially expressed genes using RNA-seq data from resting WT and *Mt3*^{-/-} BMDMφ (NCBI SRA: PRJNA533616) (19) FDR, false detection rates. **(B, C)** Heat map (left) and table (right) show differentially expressed IFN-related genes in resting *Mt3*^{-/-} BMDMφ compared to resting WT BMDMφ obtained from RNA-seq analysis. **(D)** Western blots of pIRF3, pSTAT1, STAT1, GBP2 and GBP5 in vehicle or iLPS (10 μg/ml)-treated WT and *Mt3*^{-/-} BMDMφ lysates, 3-4 independent experiments, one-way ANOVA. **(E)** Western blots of TRIF in lysates from WT and *Mt3*^{-/-} BMDMφ stimulated as above, 3 independent experiments, one-way ANOVA. **(F)** Scramble and *Ticam1* siRNA treated WT and *Mt3*^{-/-} BMDMφ treated with iLPS (10 μg/ml) or vehicle for 48h. Immunoblots of TRIF (2 independent experiments), pro-caspase-11, and active-caspase-11 in lysates and active-IL-1β in supernatants, 3 independent experiments, one-way ANOVA, data are mean ± SEM. *p < 0.05, **p < 0.01, ***p < 0.001; NS, not significant.

generated mice specifically lacking MT3 in myeloid cells (*Lys2Cre Mt3^{fl/fl}*) (**Figure 4A** and **Supplementary Figures S4A, B**). Genotyping analysis of BMDMφ and peritoneal Mφ (PMφ) from *Lys2Cre*, *Mt3^{fl/fl}* and *Lys2Cre Mt3^{fl/fl}* mice demonstrated efficient removal of the *Mt3* gene from BMDMφ and PMφ only in *Lys2Cre Mt3^{fl/fl}* mice (**Figure 4B**). To determine if myeloid MT3 deficiency augmented non-canonical inflammasome activation *in vivo*, we infected *Lys2Cre* and *Lys2Cre Mt3^{fl/fl}* mice *i.p.* with *E. coli*. After 6h,

caspase-11 inflammasome targets and bacterial burden were examined in kidney and blood. *Lys2Cre Mt3^{fl/fl}* mice exerted increased activation of caspase-11, GSDMD (N-terminal), caspase-1, and IL-1β in kidney homogenates and improved bacterial elimination compared to *Lys2Cre* control mice (**Figures 4C, D**). Thus, myeloid MT3 facilitates subversion of non-canonical inflammasome activation and contributes to antibacterial immunity *in vivo*.

MT3 Exerts a Brake on the TRIF-IRF3-STAT1 Axis to Curtail Caspase-11 Signaling

Signaling *via* the TRIF pathway is crucial for caspase-11 activation and synergistic engagement of the NLRP3 inflammasome leading to activation of caspase-1 and IL-1 β (20). Downstream of TRIF, IRF3 and IRF7 induce IFN β production that activates STAT1 signaling and promotes transcription of inflammasome components including caspase-11 and guanylate binding proteins (GBPs). GBP2 and GBP5 facilitate LPS release into the cytosol from intracellular vacuoles containing bacteria (39, 40). Our functional enrichment data based on protein-protein interaction network analyses revealed a potential involvement of MT3 in LPS, TRIF, type-I IFN and IL-1 signaling (Table 1, Supplementary Table S1 and Supplementary Files S1, S2). We further examined our published RNA-seq data (NCBI SRA: PRJNA533616) to determine differentially expressed genes by comparing resting WT and *Mt3*^{-/-} BMDM ϕ (19). The derived list of differentially expressed genes significantly enriched 12 GO BP categories directly related to cytokine and chemokine signaling and regulation of inflammatory responses based on DAVID functional enrichment analysis (Figure 5A) (41). These analyses suggested that MT3 deficiency perturbed the expression of immune-related genes even at the resting state. We reported that a lack of MT3 augments IFN γ responsiveness (19). Herein, from our RNA-seq analysis, we identified 20 genes related to IFN-signaling that were upregulated in resting *Mt3*^{-/-} BMDM ϕ compared to resting WT BMDM ϕ (p adj <0.05) (Figures 5B, C). Among these, *Isg15*, *Mx1* and *Ifit* (*Ifit1bl1*, *Ifit3*, *Ifit3b*, *Ifit2*, *Ifit1*, *Ifit1bl2*) family of genes are known targets of type-I IFNs (42–45). These observations led us to posit that MT3 regulated the cellular response to LPS challenge by modulating the TRIF-IRF3-STAT1 axis upstream of non-canonical inflammasome activation. LPS engages the TRIF-IRF3-STAT1 axis *via* toll-like receptor 4 (TLR4) signaling in M ϕ . To address this hypothesis, we challenged WT and *Mt3*^{-/-} BMDM ϕ with iLPS or vehicle and examined activation of the TRIF-IRF3-STAT1 pathway. M ϕ lacking MT3 exerted increased activation of phospho-IRF3 (pIRF3), pSTAT1, GBP2 and GBP5 (Figure 5D). TRIF protein levels were unaltered by MT3 deficiency (Figure 5E). Type-I IFN signaling is required for activation of the caspase-11 inflammasome cascade by gram-negative bacteria (20). As MT3 deficiency augmented the expression of genes involved in IFN signaling (Figures 5B, C), we blocked the interferon- α/β receptor (IFNAR) 1 using a monoclonal antibody prior to iLPS challenge in WT and *Mt3*^{-/-} M ϕ . IFNAR1 blockade resulted in decreased pro-caspase-11 (p43 subunit). Total STAT1 and pro-caspase-1 (p38 subunit) were not greatly affected (Supplementary Figure S5). We found robust attenuation of pSTAT1, active-caspase-11 and active-caspase-1, but secretion of active-IL-1 β in both WT and *Mt3*^{-/-} M ϕ was increased upon blockade of IFNAR1 signaling. This finding corresponded with high pro-IL-1 β levels in M ϕ treated with the IFNAR1 antibody (Supplementary Figure S5). These data indicate that although IFNAR1 signaling is required for fueling the non-canonical inflammasome cascade and activation of caspase-1, pro-IL-1 β and its activation are suppressed by IFNAR1.

We queried if MT3 exerted a brake on TRIF signaling to downmodulate non-canonical inflammasome activation. WT

and *Mt3*^{-/-} BMDM ϕ were treated with scramble or *Ticam1* (gene encoding TRIF) siRNA, and challenged with iLPS (Figure 5F). *Ticam1* silencing reversed the effects of MT3 deficiency resulting in a sharp reduction in caspase-11 and IL-1 β activation in M ϕ (Figure 5F). These data reveal a central role for MT3 in attenuating the crosstalk between TRIF signaling and the caspase-11 activation cascade.

Zn²⁺ Flux by MT3 Drives Suppression of the Non-Canonical Inflammasome in M ϕ

MTs are master regulators of intracellular Zn²⁺ availability and distribution (46, 47). We determined if negative control of the non-canonical inflammasome by MT3 was Zn²⁺-dependent. First, we systematically assessed Zn²⁺ changes in WT and *Mt3*^{-/-} BMDM ϕ upon challenge with iLPS over time using SEC-ICP-MS. Activation of the non-canonical inflammasome in WT M ϕ was associated with profound changes in the intracellular Zn²⁺ pool. iLPS exposure led to a gradual increase in total Zn²⁺ largely associated with the chromatogram peak(s) between 18–21 min. that we previously identified as MTs (Figures 6A, B) (9, 11). The time-dependent elevation in Zn²⁺ corresponded with kinetics of *Mt3* induction (Figures 1A and 6A, B). M ϕ lacking MT3 failed to elevate total Zn²⁺ and MT-associated Zn²⁺ in response to iLPS (Figure 6B). In contrast to the increase in Zn²⁺ pool observed in WT M ϕ challenged with iLPS, resting *Mt3*^{-/-} M ϕ harbored higher Zn²⁺ content that reduced over time post iLPS challenge (Figure 6B). These data indicate that MT3 drives an elevation in intracellular Zn²⁺ in M ϕ during non-canonical inflammasome activation.

Zn²⁺ chelation in human monocytes increases IRF3 activation (48). We reasoned that if the effects of MT3 were Zn²⁺ dependent, altering the intracellular Zn²⁺ concentration will at least in part reverse the heightened non-canonical inflammasome signaling observed in *Mt3*^{-/-} cells. To test this postulate, we exposed WT and *Mt3*^{-/-} BMDM ϕ to increasing amounts of ZnSO₄ and challenged them with iLPS *in vitro*. Exogenous ZnSO₄ supplementation remarkably reduced the ability of *Mt3*^{-/-} M ϕ to respond to iLPS. pIRF3, pSTAT1 and activation of caspase-11 were reduced in ZnSO₄-supplemented *Mt3*^{-/-} M ϕ (Supplementary Figure S6A). A similar effect of Zn²⁺ was also observed in WT M ϕ (Supplementary Figure S6A). We investigated if exposing WT M ϕ to a Zn²⁺-deficient environment would mimic the effects MT3 deficiency on the non-canonical inflammasome. WT BMDM ϕ were cultured in Zn²⁺-sufficient or Zn²⁺-deficient Opti-MEM media prior to iLPS exposure. WT M ϕ exposed to a Zn²⁺-deficient milieu manifested higher pIRF3 and caspase-11 activation accompanied by increased activation and release of IL-1 β (Figure 6C). The amount of TRIF, pro-caspase-11 and pro-IL-1 β were not affected by Zn²⁺ deficiency (Figures 6C and Supplementary Figure S6B).

Next, we directly addressed whether Zn²⁺ is required for the suppressive function of MT3 on the caspase-11 inflammasome. We first overexpressed the MT3 gene in *Mt1*^{-/-}*Mt2*^{-/-} M ϕ and isolated the protein. *Mt1*^{-/-}*Mt2*^{-/-} BMDM ϕ were transfected with the *Mt3* overexpressing vector (pCMV6-Ac-MT3-GFP) or an empty vector (pCMV6-Ac-GFP) control. *Mt1*^{-/-}*Mt2*^{-/-} M ϕ were

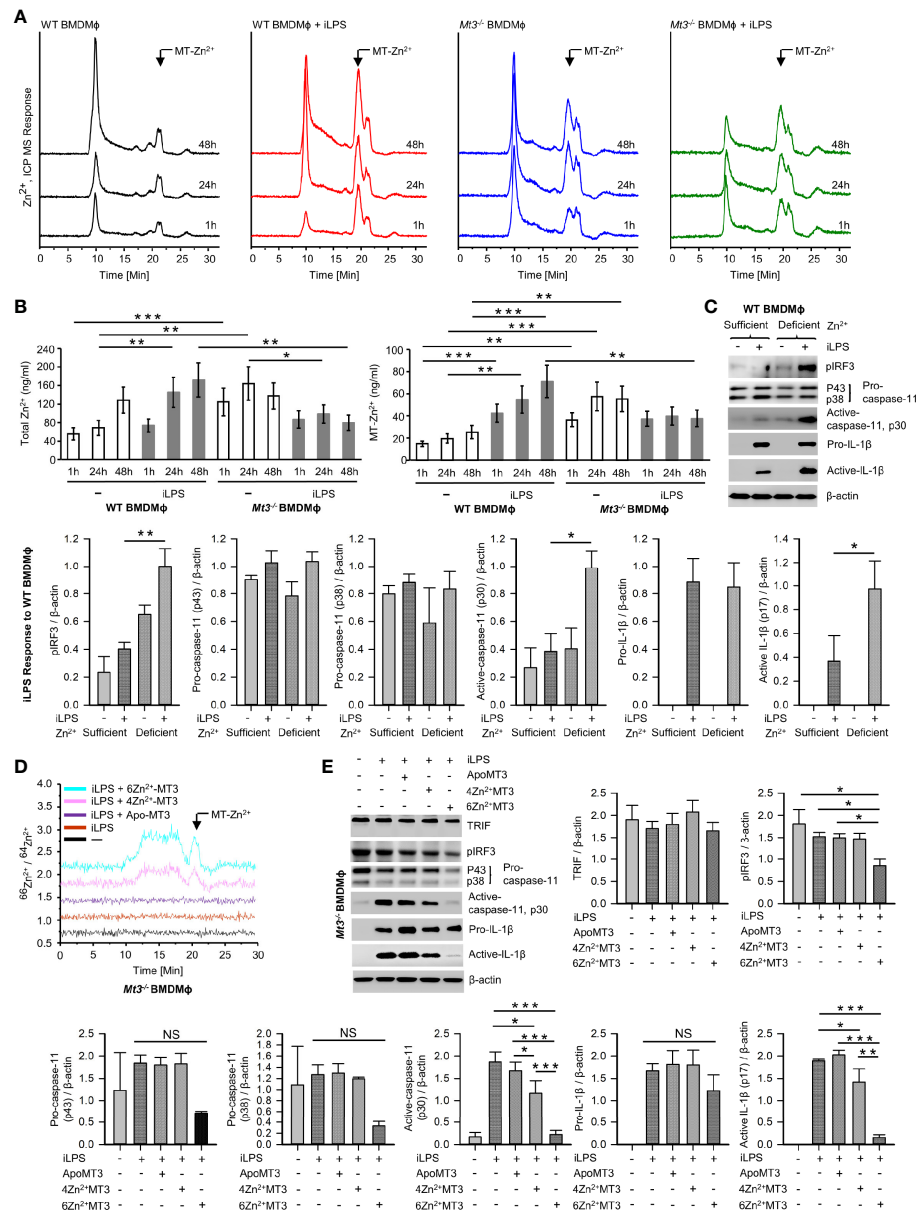


FIGURE 6 | See also **Supplementary Figures S6, 7** MT3-Zn²⁺ axis drives negative regulation of the non-canonical inflammasome. **(A)** SEC-ICP-MS of WT and *Mt3*^{-/-} BMDMφ exposed to vehicle or iLPS (10 μg/ml) for the indicated time points, chromatograms depict Zn²⁺ distribution in cell lysates across various molecular masses, arrow indicates Zn²⁺ associated with the MT-peak (18-21 min.) on the chromatogram, Y axis is off-set to allow easy comparison under the same scale. **(B)** Bar graphs of total Zn²⁺ and MT-Zn²⁺ in WT and *Mt3*^{-/-} BMDMφ post iLPS (10 μg/ml) or vehicle exposure. Two-way t-test against respective BMDMφ controls at each time point, 3 independent experiments, data are mean ± SD. **(C)** WT BMDMφ treated with iLPS (10 μg/ml) or vehicle for 24h in Zn²⁺ sufficient or Zn²⁺ deficient Opti-MEM media, immunoblots of pIRF3, pro-caspase-11, active-caspase-11 and pro-IL-1β in lysates and active-IL-1β in media supernatants, one-way ANOVA, data are mean ± SEM. **(D, E)** *Mt3*^{-/-} BMDMφ transfected with Pro-Ject™ or Pro-Ject™ complexed with apo-MT3, 4Zn²⁺MT3 or 6Zn²⁺MT3 and treated with iLPS (10 μg/ml) or vehicle for 24h in Zn²⁺ deficient Opti-MEM media. **(D)** Chromatograms depict Zn²⁺ distribution in cell lysates across various molecular masses, arrow indicates Zn²⁺ signal associated with the MT-peak (18-21 min.) on the chromatogram, Y axis is off-set to allow easy comparison under the same scale. **(E)** Western blots of pIRF3, pro-caspase-11, active-caspase-11 and pro-IL1β in lysates and active-IL-1β in supernatants, 3 independent experiments, one-way ANOVA, data are mean ± SEM. *p < 0.05, **p < 0.01, ***p < 0.001; NS, not significant.

used so as to exclude any contribution of these MTs in the MT3 purification process. The MT-associated peak from MT3-overexpressed Mφ was identified by SEC-ICP-MS (**Supplementary Figure S7**) and collected. We complexed

MT3 with the ⁶⁶Zn²⁺ isotope to acquire an MT3-Zn²⁺ saturation of 4 Zn²⁺ ions per MT3 (MT3-4Zn²⁺) and 6 Zn²⁺ ions per MT3 (MT3-6Zn²⁺). The ⁶⁶Zn²⁺ isotope was used to monitor changes in the ratio of ⁶⁶Zn²⁺/⁶⁴Zn²⁺ post-transfection

of the MT3- $^{66}\text{Zn}^{2+}$ complexes in M ϕ . We transfected apo-MT3, MT3-4Zn $^{2+}$ or MT3-6Zn $^{2+}$ into *Mt3* $^{-/-}$ BMDM ϕ in Zn $^{2+}$ -deficient media. The use of *Mt3* $^{-/-}$ BMDM ϕ and Zn $^{2+}$ -deficient media enabled exclusion of any possible contribution from endogenous MT3 and exogenous Zn $^{2+}$ in our analysis. Post-transfection of apo-MT3 or MT3-Zn $^{2+}$ complexes, M ϕ were challenged with iLPS to activate the non-canonical inflammasome. To confirm that intracellular Zn $^{2+}$ changes occurred upon transfection of the MT3- $^{66}\text{Zn}^{2+}$ complexes, we analyzed BMDM ϕ lysates by SEC-ICP-MS. *Mt3* $^{-/-}$ cells transfected with MT3-4Zn $^{2+}$ and MT3-6Zn $^{2+}$ but not apo-MT3 exhibited an increase in the $^{66}\text{Zn}^{2+}/^{64}\text{Zn}^{2+}$ ratio in the MT-peak region at 18–21 mins. in the chromatogram indicating an elevation in the intracellular $^{66}\text{Zn}^{2+}$ isotope (**Figure 6D**). These data confirm that transfection of the MT3-Zn $^{2+}$ complexes resulted in an increase in intracellular $^{66}\text{Zn}^{2+}$ in M ϕ . In parallel, we isolated cell lysates and supernatants proteins from these M ϕ to determine whether apo-MT3 or the MT3-Zn $^{2+}$ complexes modulated the non-canonical inflammasome pathway. Transfection of MT3-4Zn $^{2+}$ and MT3-6Zn $^{2+}$ but not apo-MT3, dampened pIRF3, active caspase-11 and active IL-1 β in response to iLPS (**Figure 6E**). TRIF levels were unaffected by MT3 transfection (**Figure 6E**). Pro-caspase-11 and pro-IL-1 β were modestly diminished by MT3-4Zn $^{2+}$ and MT3-6Zn $^{2+}$ exposure, but these changes were not significant (**Figure 6E**). The effect of MT3-6Zn $^{2+}$ was more profound than that of MT3-4Zn $^{2+}$ indicating that a higher Zn $^{2+}$ saturation on MT3 corresponded with a stronger suppressive effect on the non-canonical inflammasome (**Figure 6E**).

Taken together, these findings reveal a previously undescribed interplay between the non-canonical inflammasome and its negative regulator, whereby the MT3-Zn $^{2+}$ axis suppresses caspase-11 inflammasome, but the two molecules concur in compromising immunological fitness of the host during bacterial pathogenesis.

DISCUSSION

Human CASPASE-4 or mouse caspase-11 are inflammatory caspases that drive cell death *via* pyroptosis. These caspases directly recognize bacterial LPS in the cytosol resulting in CASPASE-4 or caspase-11 auto-processing and synergistic activation of the NLRP3 inflammasome that culminates in caspase-1 activation, processing and release of IL-1 β and IL-18 (2, 32). While the non-canonical inflammasome boosts host immunological fitness to some bacterial infections, heightened activation of this cascade poses the danger of tissue injury and organ failure. Thus far, negative regulation of IFN β production by prostaglandin E2, immunity-related GTPases M clade, cyclic-adenosine monophosphate, and low dose oxidized phospholipid oxPAPC have been shown to thwart activation of the non-canonical inflammasome (49–52). The role of MTs in regulating inflammasome activation pathways has largely been unknown. Herein, we identify a previously undescribed function

of MT3 in curtailing the highly inflammatory non-canonical inflammasome activation cascade *via* Zn $^{2+}$ regulation. We demonstrate that while MT3 orchestrates negative regulation of the caspase-11 inflammasome, the combined presence of MT3 and caspase-11 blunts resistance to *E. coli* infection *in vivo*. These studies illuminate a central role for the MT3-Zn $^{2+}$ axis in shaping the intricate balance between host antibacterial immunity and unrestrained inflammation.

MT1 and MT2 are ubiquitously expressed and can be induced by infection (53–56). Initial studies on MT3 revealed tissue-restricted expression with high levels predominantly found in the brain tissue where it inhibits neuronal cell death (21, 57). The immunological functions of MT3, particularly in the innate arm have only recently been investigated (11, 19, 21). We reported that *Mt3* is inducible by the pro-resolving cytokines IL-4 and IL-13 in M ϕ . One inducer of *Mt3* expression is STAT6 signaling, and this MT is crucial in shaping the phenotypic and metabolic attributes of M ϕ stimulated with type-2 cytokines (11, 19). Studies on MTs in response to exogenous LPS stimulation have largely focused on MT1 and MT2. Monocytes and M ϕ induce MT1 and MT2 upon extracellular LPS exposure (58, 59). We found that iLPS challenge also induced *Mt1* and *Mt2* in M ϕ , although their expression receded to baseline over time. In contrast, *Mt3* expression gradually increased as non-canonical inflammasome activation progressed. Subversion of inflammatory responses in M ϕ by MT3 and the delayed expression pattern in response to a non-canonical inflammasome trigger are reminiscent of waning inflammation after the initial peak of inflammasome activation has subsided (19). In line with this hypothesis, protein interaction network analysis predicted the involvement of MT3 in cellular responses related to non-canonical inflammasome activation. M ϕ lacking MT3 exerted robust activation of caspase-11, caspase-1 and IL-1 β . Similar to our observations with mouse MT3, a lack of human MT3 exacerbated the activation of CASPASE4 and IL-1 β in hM ϕ . Human and mouse MT3 proteins that share 86% identity thus have consistent roles that culminate in negative regulation of the non-canonical inflammasome cascade in M ϕ (60). As non-canonical inflammasome activation progressed, MT3 guarded against its unrestrained activation to avert potential inflammatory damage. Together, these observations reveal a pivotal role for MT3 in curtailing the vigor of the caspase-11 activation cascade. Although *Mt3* $^{-/-}$ mice exerted higher sepsis scores and weight loss, they succumbed to septic shock similar to WT controls, suggesting that a threshold level of caspase-11 activation may be sufficient to promote sepsis-associated mortality.

In vivo, LPS released from OMV of gram-negative bacteria triggers caspase-11 activation (2, 3). Myeloid-MT3 contributed to averting excessive activation of caspase-11 and synergistic activation of the canonical inflammasome in response to gram-negative microbial triggers. MT3 compromised antibacterial resistance to *E. coli* and *K. pneumoniae*, but this was not due to its suppressive action on the caspase-11 inflammasome *in vivo*. Instead, *Mt3* $^{-/-}$ and *Casp-11* $^{-/-}$ mice manifested improved antibacterial immunity, an effect that was further augmented when *Mt3* $^{-/-}$ mice lacked caspase-11. The synergism between MT3 and caspase-11 may result from

independent or combined effects of MT3 and caspase-11 *in vivo*. Of note, the activation of caspase-1 and caspase-8 in the absence of MT3 and caspase-11 reveal that canonical inflammasome activation was operational and both caspase-1 and caspase-8 may contribute to IL-1 β activation *in vivo* (38).

M ϕ utilize Zn²⁺ deprivation and Zn²⁺ intoxication mechanisms as strategies for antimicrobial defense (56, 61, 62). We previously showed that ablation of MT3 in M ϕ augments immunity to *Histoplasma capsulatum* as well as *E. coli*. The increased antimicrobial resistance in *Mt3*^{-/-} M ϕ is at least partially attributable to a decrease in the M ϕ exchangeable Zn²⁺ pool and exaggerated IFN γ responsiveness (11, 19). Myeloid and non-myeloid cells may together contribute to bacterial elimination in whole-body MT3-deficient mice. Nonetheless, the augmented bacterial elimination observed in *Lys2Cre Mt3*^{fl/fl} mice indicates that myeloid-MT3 contributes to the suppression of antibacterial defenses *in vivo*. The finding that MT3 deficiency dually bolstered inflammasome activation and antibacterial immunity underpins a role for this protein in suppressing the emergence of a proinflammatory phenotype in M ϕ . Our data unveil a unique crosstalk between caspase-11 and its negative regulator, whereby although MT3 keeps caspase-11 activation under control, the two synergistically compromise host immunological fitness to gram-negative bacterial infection.

Caspase-11 activation can have opposing effects on clearance of different bacteria. It improves resistance to *Burkholderia thailandensis*, *B. pseudomallei*, *Brucella abortus*, and *Legionella pneumophila* but may compromise immunity to *B. cenocepacia*, *Salmonella typhimurium*, *E. coli*, *Shigella flexneri*, *K. pneumoniae* and gram-positive infections including *Streptococcus pyogenes*, *Staphylococcus aureus* and *Listeria monocytogenes* (28, 31–33, 35, 63–69). Lipoteichoic acid from gram-positive bacteria engages the caspase-11 inflammasome *via* NLRP6 (28). Likewise, GAS infection led to caspase-11 activation *in vivo*. Although MT3 exerted disparate effects on caspase-11 activation in gram-positive and gram-negative infections, caspase-1 and IL-1 β activation was suppressed by MT3 in both infection settings. In the context of GAS infection, both the host and the pathogen contribute to canonical inflammasome activation. Surface and secreted GAS virulence factor *emm*, and the streptococcal pyrogenic exotoxin B (SpeB) proteins act as second signals to activate caspase-1 signaling (70–72). Our data do not exclude the role of pathogen-derived factors in contributing to the increased canonical inflammasome activation observed in *Mt3*^{-/-} mice infected with GAS. Nonetheless, our findings indicate that MT3 exerted a suppressive effect on the canonical caspase-1 pathway activated by gram-positive bacteria, while sparing negative regulation of the upstream non-canonical inflammasome activation *in vivo*.

The TRIF pathway is a central node in activation of the caspase-11 inflammasome in response to gram-negative infection (20). Targeting TRIF, but not IFNAR1, completely reversed the inflammatory cascade, including IL-1 β activation. Blockade of IFNAR1 attenuated downstream activation of STAT1, caspase-11 and caspase-1, but both pro-IL-1 β and

active IL-1 β levels were dramatically enhanced. This finding contrasts with the previously reported requirement of both TRIF and IFNAR1 in this pathway (20). Although that study utilized BMDM ϕ from *IFNAR1*^{-/-} mice and we used an anti-IFNAR1 monoclonal antibody, both approaches resulted in attenuation of targets downstream of IFNAR1. Emerging evidence points to an indirect inhibitory effect of type-I IFNs on inflammasome activation by decreasing pro-IL-1 β transcription *via* IL-10 or 25-hydroxycholesterol (73, 74). The subdued activation of caspase-1 and heightened active IL-1 β levels suggests that IL-1 β activation occurs *via* a caspase-1 independent pathway when IFNAR is blocked. Interfering with IFNAR1 signaling can therefore subdue activation of critical inflammasome components including caspase-11 and caspase-1 but sustain IL-1 β production and activation.

The crucial function of Zn²⁺ as a signaling molecule is well documented (13, 75–77). Changes in plasma and cellular Zn²⁺ levels regulate the production of various cytokines *via* NF- κ B signaling (78, 79). Specifically, Zn²⁺ deficiency in humans increases the production of tumor necrosis factor (TNF) α and IL-1 β by LPS-treated PBMCs *ex vivo*, whereas Zn²⁺ supplementation reduces it (80, 81). Therefore, a shift from physiological Zn²⁺ concentrations at the systemic or cellular level can impact proinflammatory cytokine responses and inflammation. To our knowledge, modulation of M ϕ Zn²⁺ homeostasis during non-canonical inflammasome activation has not been previously demonstrated. Our data show that caspase-11 activation is accompanied by a gradual expansion of the intracellular Zn²⁺ pool driven by MT3. Zn²⁺ deficiency did not augment pro- forms of caspase-11 (p43 and p38), but specifically increased their activation. Zn²⁺ diminishes signaling *via* IRF3 by limiting its nuclear localization (48). Accordingly, MT3 interfered with signaling *via* the TRIF-IRF3-STAT1 axis by shaping the M ϕ Zn²⁺ pool. The MT3-Zn²⁺ axis dampened IRF3 phosphorylation and downstream mediators without impacting TRIF levels. Although we cannot rule out the direct effect of Zn²⁺ on inflammasome components downstream of IRF3, the suppressive action of MT3 on the non-canonical inflammasome was Zn²⁺ dependent. Our data demonstrate that by manipulating the M ϕ Zn²⁺ milieu, caspase-11 activation can either be triggered or averted. This finding has important implications in defining a role for Zn²⁺ in subverting caspase-11 driven hyperinflammation. Developing therapeutic strategies that temper activation of the caspase-11/4 inflammasome have garnered tremendous interest to alleviate endotoxemia. In light of this, the MT3-Zn axis emerges as a fresh and vital candidate that guards the vigor of a caspase-11 fueled inflammatory response. In the context of gram-negative bacterial pathogenesis, our data indicate that strategies aimed at combined targeting of MT3 and the caspase-11 inflammasome may be more beneficial in infection control than targeting caspase-11 alone.

Taken together, our studies illuminate a double-edged phenomenon in inflammasome regulation whereby the MT3-Zn²⁺ axis is a sentinel of the caspase-11 inflammasome but MT3 and the non-canonical inflammasome function in concert to compromise host antibacterial resistance.

MATERIAL AND METHODS

Reagents and Resources

Reagents and resources can be found in **Table 2**.

TABLE 2 | Reagents and resources.

Name	Source	Identifier
Antibodies		
anti-TRIF	Proteintech	Cat#23288-1-AP
anti-pIRF3 (Ser396)	BIOSS	Cat#bs-3195R
anti-STAT1	Abcam	Cat#ab99415
anti-pSTAT1 (pY701) [M135]	Abcam	Cat#ab29045
anti-GBP5	Proteintech	Cat#13220-1-AP
anti-GBP2	Proteintech	Cat#11854-1-AP
anti-Caspase 11 (17D9)	eBioscience™	Cat#14-9935-82
anti-Caspase-11	Abcam	Cat# ab180673
anti-CASPASE-4	MBL	Cat#M029-3
anti-GSDMD	Proteintech	Cat#20770-1-AP
anti-Caspase-1	AdipoGen Life Sciences	Cat#AG-20B-0042-C100
anti-Caspase-1 (14F468)	Santa Cruz Biotechnology	Cat#sc-56036
anti-IL-1β/IL-1F2	R&D Systems	Cat#AF-401-NA
anti-IL-1β/IL-1F2	R&D Systems	Cat#MAB4011
anti-IL-1β (B122)	Santa Cruz Biotechnology	Cat#sc-12742
anti-Caspase-8 (1G12)	Enzo Life Sciences	Cat#ALX-804-447-C100
anti-β-actin	Cell Signaling Technology	Cat#4967s
anti-β-actin	ThermoFisher Scientific	Cat#PA1-183
anti-β-actin	R&D Systems	Cat#MAB-8929
Mouse anti-armenian hamster IgG-HRP	Santa Cruz Biotechnology	Cat#sc-2789
Goat anti-rabbit IgG(H+L), HRP conjugate	Proteintech	Cat#SA00001-2
IRDye® 800CW goat anti-rabbit IgG	LI-COR Biosciences	Cat#926-32211
IRDye® 680RD goat anti-rabbit IgG	LI-COR Biosciences	Cat#926-68071
Goat anti-mouse IgG(H+L), HRP conjugate	Proteintech	Cat#SA00001-1
IRDye® 680RD goat anti-mouse IgG	LI-COR Biosciences	Cat#926-68070
Mouse IgG (H&L) secondary antibody peroxidase conjugated pre-adsorbed	Rockland Immunochemicals	Cat#610-1319-0500
Rabbit anti-goat IgG(H+L), HRP conjugate	Proteintech	Cat#SA00001-4
Goat anti-Rat IgG(H+L), HRP conjugate	Proteintech	Cat#SA00001-15
IRDye® 800CW goat anti-rat IgG	LI-COR Biosciences	Cat#926-32219
anti-IFNAR1 (Clone: MAR1-5A3)	BioLegend	Cat#127302
anti-IgG1 (Clone: MOPC-21)	BioLegend	Cat#400102
Bacterial Strains		
<i>Escherichia coli</i> (K12)	Dr. Jason Gardner (gardnejr@ucmail.uc.edu)	N/A
<i>Klebsiella pneumoniae</i> (KP2 2-70)	Dr. Jason Gardner (gardnejr@ucmail.uc.edu)	N/A
Group A Streptococcus (<i>Streptococcus pyogenes</i>)	Dr. Suba Nookala (suba.nookala@und.edu)	N/A

(Continued)

TABLE 2 | Continued

Name	Source	Identifier
Primers		
<i>Mt3</i>	Applied Biosystems	Mm00496661_g1
<i>Mt2</i>	Applied Biosystems	Mm00809556_s1
<i>Mt1</i>	Applied Biosystems	Mm00496660_g1
<i>Hprt</i>	Applied Biosystems	Mm00446968_m1
<i>MT3</i>	Applied Biosystems	Hs00359394_g1
<i>MT2A</i>	Applied Biosystems	HS02379661_g1
<i>HPRT1</i>	Applied Biosystems	Hs99999909_m1
Genotyping Primers	IDT	N/A
siRNA and expression vector		
<i>MT3</i>	Ambion	Cat#AM16708
<i>Ticam1</i>	Dharmacon™	Cat#L-055987-00-0005
ON-TARGETplus™ Control Pool (Non-Targeting pool)	Dharmacon™	Cat#D-001810-10-20
pCMV6-AC-GFP (PS100010)	ORIGENE	Cat#MG200059
pCMV6-AC-GFP	ORIGENE	Cat# PS100010
Chemicals and accessories		
RPMI 1640	CORNING	REF#10-041-CV
Opti-MEM® I	GIBCO	REF#31985-070
FBS	HyClone	Cat#SH30396.03
DPBS	CORNING	REF#21-031-CV
PBS without calcium and magnesium	CORNING	REF#21-040-CV
HBSS	CORNING	REF#21-021-CM
HEPES	Sigma	Cat#H3375
Mouse M-CSF	PEPROTECH	Cat#315-02
Human M-CSF	PEPROTECH	Cat#300-25
Trypsin-EDTA	CORNING	REF#25-053-CI
LPS-B5 Ultrapure	InVivoGen	Cat#tlrl-pb5lps
Glycerol	Fisher Bioreagents	Cat#BP229-1
LB Broth	Fisher Bioreagents	Cat#BP1427-500
BBL™ Brain Heart Infusion Broth	Becton Dickinson	Cat#22182
Agar	BD Bacto™	Cat#214010
BD Bacto™ Dehydrated Culture Media: Todd Hewitt Broth	BD	Cat#249240
Gibco™ Bacto™ Yeast Extract	Gibco	Cat#212750
BD BBL™ RODAC™ Trypticase™ Soy Agar with 5% Sheep Blood (TSA II)	BD	Cat#221261
EZ Pack™ Agarose	ASi	Item No.#AG2501
MCC950	ApexBio	B7946-50
ZnSO ₄	Sigma	Cat#z-4750
Sodium Chloride	Sigma	Cat#S1679-1KG
Ethyl Alcohol	Fisher Scientific	Cat#A407-4
Methanol	Fisher Scientific	Cat#A434-20
Methanol	BDH	Cat#BDH1135-4LP
Dimethyl Sulfoxide	Sigma	Cat#D8418-1L
Chloroform	Fisher Scientific	Cat#C5312
Hydrochloric Acid	Fisher Scientific	Cat#A508-212
Sulfuric Acid	Fisher Scientific	Cat#A300 ^{SI} -212
Sodium Hydroxide	Fisher Scientific	Cat#S318-3
Precise Protein Gels	Invitrogen	REF#XP04205BOX
SurePAGE™, Bis-Tris, 10x8 gels (4-20%, 15 wells)	GenScript	Cat#M00657
Tris-MOPS-SDS Running Buffer Powder	GenScript	Cat#M00138
Nitrocellulose membranes	BIO-RAD	Cat#162-0112

(Continued)

TABLE 2 | Continued

Name	Source	Identifier
Protease & Phosphatase Inhibitor Cocktail	Thermo Scientific	Cat#78442
Denaturing Cell Extraction Buffer	Invitrogen	Cat#FNN0091
XCell II™ Blot Module	ThermoFisher Scientifics	Cat#EI9051
Glycine	Fisher Scientific	Cat#BP381
Tris-base	Fisher Scientific	Cat#BP152
SDS	Fisher Scientific	Cat#BP166
Tween 20	Acros Organics	Cat#23336-0010
Tween 20	Sigma	Cat#P-1379
Triton X100	Fisher Scientific	Cat#BP151
Bovine serum albumin	Sigma	Cat#A7030
Intercept® (TBS) Blocking Buffer	LI-COR Biosciences	Cat#927-60001
Non-fat dry milk	Nash Finch Co.	N/A
Isoflurane	Covetrus	NDC Code(s) #11695-6777-2
Nair	Chuech & Dwight Co. inc	N/A
Gauze	Medline	REF#PRM25444
Puritan cotton tipped applicator	Puritan	SKU#836-WC
Insulin injection syringe (1mL)	Exelint international co.	Cat#26029
1 ml plastic Syringe	Fisherbrand	Cat#14955459
1 ml plastic Syringe	Fisherbrand	Cat#14955456
BioLite12 well multidish	Thermo Scientific	Lot# H4XA4RE106
24 well tissue culture plates	CellPro	Lot# 072219BA03
48 well cell culture plate	NEST	Lot# 121717A004
Tissue culture plate 96 well, flat bottom	Fisherbrand	Cat#FB012931
96 well ELISA plate	NEST	Lot#04291818A007
Petri dish	NEST	Lot#753001
15 ml Centrifuge tube	Fisher Scientific	Cat#14-955-237
50 ml Centrifuge tube	Fisher Scientific	Cat#14-955-239
Cell scraper	SPL Life Sciences	Cat#90030
Golden Rod animal Lancet (4mm)	Medipoint Inc	N/A
Omni homogenizer Th-01 and tips	Omni International	Model Number#THP115
GeneArt Platinum Cas9	ThermoFisher	Cat# B25641
Nuclease	ThermoFisher	Cat# 1074181
Alt-R SpCas9 Nuclease 3NLS sgRNA	CCHMC transgenic core	N/A
TSK gel 3000SW gel filtration column	TOSOH BIOSCIENCE	Cat#05789
DreamTaq DNA Polymerase	Thermo Scientific	REF#EP0702
Commercial Assays		
TransIT®-TKO	Mirus Bio LLC	Prod. No.#MIR 2150
TransIT®-LT1	Mirus Bio LLC	Prod. No.#MIR 2300
Pierce Protein Transfection Reagent Kit	Thermo Scientific	REF#89850
Human IL-1β/IL-1F2 DuoSet ELISA	R&D Systems	Cat#DY201-05
Mouse IL-1β	BioLegend	Cat# 432601
IL-1α	BioLegend	Cat# 433401
RNeasy Mini Kit	Qiagen	Cat# 74104
QUICK-RNA™ MINIPREP KIT	Denville Scientific	Cat# R1055
Reverse Transcription System	Promega	REF#A3500
Probe Lo-Rox 2X qPCR Mix	RADIANT™	Cat#QP9020
CytoTox 96® NonRadioactive Cytotoxicity Assay kit	Promega	REF#G1781

(Continued)

TABLE 2 | Continued

Name	Source	Identifier
SuperSignal™ West Femto Maximum Sensitivity Substrate	Thermo Scientific	Cat#34096
NEBNext Poly(A) mRNA Magnetic Isolation Module	New England BioLabs	Cat#E7490L
NEBNext Ultra Directional RNA Library Prep Kit	New England BioLabs	Cat# E7420L
NEBNext Library Quant Kit	New England BioLabs	Cat# E7630L
MEGAshorscript T7 Kit	Thermo Fisher	Cat#AM1354
MEGAclear Kit	Thermo Fisher	Cat# AM1908
Quick-DNA™ Miniprep Plus Kit	ZYMO RESEARCH	Cat#D4069
Radiant™ Taq DNA Polymerase	RADIANT™	Cat#C101
Experimental Models: Organisms/Strains		
C57BL/6 Mice	Jackson Laboratory	Stock#00064
C57BL/6 <i>Mt3</i> ^{-/-} deletion of Exon 3	Transgenic Animal and Genome editing core facility at CCHMC	N/A
C57BL/6 <i>Mt1</i> ^{-/-} <i>Mt2</i> ^{-/-}	Dr. George S. Deepe (deepegs@ucmail.uc.edu)	N/A
C57BL/6 <i>Casp4</i> ^{tm1Yuan/J} (<i>Casp-11</i> ^{-/-})	Jackson Laboratory	Stock#024698
<i>Mt3</i> ^{-/-} <i>Casp-11</i> ^{-/-}	Crossed and bred in-house	N/A
C57BL/6 <i>Lys2Cre</i>	Dr. George S. Deepe (deepegs@ucmail.uc.edu)	N/A
C57BL/6 <i>Lys2Cre Mt3</i> ^{fl/fl}	Crossed and bred in-house	N/A
Instrument, Software and Algorithms		
FluorChem® HD2	Cell Biosciences	S/N#FC HD2 Imager
Odyssey CLx Imaging system	LI-COR	N/A
7500 Fast Real Time PCR System	Applied Biosystems	S/N#275013253
RNA-seq data analysis - DAVID Bioinformatics Resources v.6.8	NIAID/NIH	(https://david.ncifcrf.gov/summary.jsp)
Protein-protein interaction networks- STRING v.11.0	ELIXIR	(https://string-db.org/)
NIH ImageJ Fiji	NIH	(https://imagej.nih.gov/ij/)

Microbes

E. coli (K12) and *K. pneumoniae* were kindly provided by Dr. Jason Gardner at the University of Cincinnati. Group A Streptococcus (GAS 5448) was kindly provided by Dr. Suba Nookala at the University of North Dakota.

Mice

All mice used in this study were on the C57BL/6 background. WT and *Casp4*^{tm1Yuan/J} (*Casp-11*^{-/-}) mice were acquired from the Jackson Laboratory. *Lys2Cre* mice were kindly provided by Dr. George S. Deepe, Jr. (University of Cincinnati). *Mt3*^{-/-} (exon 3 deleted) and *Mt3*^{fl/fl} mice were generated using clustered regularly interspaced short palindromic repeats (CRISPR) by the Transgenic Animal and Genome Editing Core facility at the Cincinnati Children's Hospital Medical Center (CCHMC). In mice, the *Mt* gene cluster is located on chromosome 8. The *Mt3*

gene consists of 3 exons and is preceded by *Mt1* and *Mt2* genes. We targeted exon 3 of *Mt3* by flanking it with loxP sites (*Mt3^{fl/fl}*) using the CRISPR-Cas9 gene targeting approach. *Lys2Cre Mt3^{fl/fl}* mice that exhibit myeloid *Mt3* deficiency were generated by crossing *Lys2Cre* mice to *Mt3^{fl/fl}* mice. Deletion of the *Mt3* gene was confirmed in BMDM ϕ and PM ϕ of *Lys2Cre Mt3^{fl/fl}* mice by genotyping as detailed in the CRISPR/Cas9 generation of *Mt3^{fl/fl}* mice section. To confirm 3' loxP site insertion or deletion, genomic DNA amplified using forward (5' TAG GCT TCC CAC CTG TTT GG 3') and reverse (5' GCC AAG ATA AAG TCC GGG GT 3') primers. To confirm 5' loxP site insertion or deletion, genomic DNA amplified using forward (5' TCG AAC TAC CTC CAA ACA GAG AAC 3') and reverse (5' TCA GTT TGG TCC AAA CGG GAT G 3') primers. To confirm *Lys2Cre* gene insertion, genomic DNA amplified using mutant (5' CCC AGA AAT GCC AGA TTA CG 3'), common (5' CTT GGG CTG CCA GAA TTT CTC 3') and WT (5' TTA CAG TCG GCC AGG CTG AC 3') primers. *Casp-11^{-/-}Mt3^{-/-}* mice were generated by crossing *Casp-11^{-/-}* mice to *Mt3^{-/-}* mice. *Casp-11* was amplified using tail genomic DNA by mutant reverse (5' CGC TTC CTC GTG CTT TAC GGT AT 3'), common forward (5' ACA ATT GCC ACT GTC CAG GT 3') and WT reverse (5' CAT TGC TGA CCT TAT TTC TGT ATG G 3') primers. *Mt3* was amplified using tail genomic DNA by forward (5' TTG GGG TGA GGT GTA GAG GT 3') and reverse (5' GCC AAG ATA AAG TCC GGG GT 3') primers. Mice used in this study had ad-libitum access to food and water. All mice were housed in the Department of Laboratory Animal Medicine, University of Cincinnati, accredited by American Association for Accreditation of Laboratory Animal Care (Frederick, MD) and experiments were conducted in accordance with Animal Welfare Act guidelines of the National Institutes of Health.

CRISPR/Cas9 Generation of *Mt3^{fl/fl}* Mice

The methods for the design of sgRNAs, donor oligos and the production of *Mt3^{fl/fl}* (loxP sites surrounding exon 3 of the murine *Mt3* gene) animals were as described previously (82). The sgRNAs were selected according to the on- and off-target scores from the CRISPR design web tool (<http://genome-engineering.org>) as well as CRISPOR (<http://crispor.tefor.net>) (83). The selected sgRNA target sequences were cloned, according to the published method (84), into the pX458 vector (addgene #48138) that was modified by us to contain an optimized sgRNA scaffold (85) and a Cas9-2A-GFP. Their editing activity were validated by the T7E1 assay in mouse mK4 cells (86), compared side-by-side with Tet2 sgRNA that was known to work in mouse embryos efficiently (87). Validated sgRNA was transcribed *in vitro* using the MEGAscript T7 kit (ThermoFisher) and purified by the MEGAclear Kit (ThermoFisher), and stored at -80°C. To prepare the injection mix, we incubated sgRNA and Cas9 protein (ThermoFisher) at 37°C for 5 mins. to form the ribonucleoprotein complex and then added the donor oligos to it. The initial attempt was to insert both loxP sites simultaneously *via* piezo-driven cytoplasmic injection (88) of 100 ng/ul Cas9 protein, 50 ng/ul 5' sgRNA, 50 ng/ul 3' sgRNA, 50 ng/ul 5' donor,

and 50 ng/ul 3' donor into fertilized eggs. Injected eggs were transferred into the oviductal ampulla of pseudo-pregnant CD-1 females on the same day. Pups were born and genotyped by PCR and Sanger sequencing. However, only 3' loxP-containing mice were obtained from this attempt. After breeding them to homozygosity for the 3' loxP, a new set of 5' sgRNA and the donor oligo was designed and injected into the zygotes with the mix containing 150 ng/ul Cas9 protein, 75 ng/ul 5' sgRNA, and 100 ng/ul ssDNA donor oligo. Injected eggs were transferred into the oviductal ampulla of pseudopregnant CD-1 females on the same day. Pups were born and genotyped by PCR and Sanger sequencing. Founder mice carrying both 5' and 3' loxP sites in cis were finally obtained. Animals were housed in a controlled environment with a 12-h light/12-h dark cycle, with free access to water and a standard chow diet. All animal procedures were carried out in accordance with the Institutional Animal Care and Use Committee-approved protocol of Cincinnati Children's Hospital and Medical Center.

M ϕ Culture

hM ϕ were prepared from peripheral blood mononuclear cells (PBMCs). Briefly, human blood obtained from the Hoxworth Blood Center, University of Cincinnati was diluted (1:2) with calcium- and magnesium-free 1X Dulbecco's phosphate-buffered saline (DPBS) and inverted gently to mix. Ficoll-Paque (10 ml for the total volume of 40 ml diluted blood) was layered at the bottom of the tube. The tubes were centrifuged at 400 X g for 30 mins. without break at 20°C. The PBMC interface was transferred to sterile tubes and washed three times using 40 ml of DPBS containing 2mM EDTA and centrifuged at 120 X g for 10 mins. without break at 4°C. A final wash was performed with DPBS (without EDTA). Isolated PBMCs were resuspended in complete RPMI 1640 medium. PBMCs (5 X 10⁶) were plated in 24 well plates containing complete RPMI medium. After 24h, adherent monocytes were washed three times with DPBS and plated in complete RPMI 1640 medium (Corning®) containing 10 ng/ml macrophage-colony stimulating factor (M-CSF), 10%FBS, 10 μ g/ml gentamycin sulfate (Alkali Scientific Inc.) and 2-mercaptoethanol. Cells were differentiated by exposure to human recombinant M-CSF on days 0, 2 and 4. After 6 days, hM ϕ were washed with DPBS prior to use for the experiment.

Mouse BMDM ϕ were prepared by differentiating bone marrow cells in complete RPMI 1640 medium containing 10 ng/ml mouse M-CSF, 10% fetal bovine serum (FBS) (HyClone Laboratories, Utah), gentamycin sulfate (10 μ g/ml) and 2-mercaptoethanol. BMDM ϕ were fed on days 0, 2 with complete RPMI 1640 medium containing 10 ng/ml M-CSF and were supplemented on day 4 with M-CSF. After 6 days, adherent M ϕ were harvested by washing with DPBS followed by trypsinization and centrifuged at 1600 rpm for 5 mins. at 4°C. M ϕ were washed again with DPBS at 1600 rpm for 5 mins. at 4°C and counted under the microscope. Dead cells were excluded from enumeration using Trypan Blue stain. BMDM ϕ (0.5 X 10⁶ in 24 well or 1 X 10⁶ in 12 well plate) were seeded.

Bioinformatics Analysis

The STRING database was used to review the protein-protein interaction networks of MT3 in *Mus musculus* and *Homo sapiens* (22). A full network analysis was conducted based on text mining, experiments, databases, co-expression, neighborhood, gene fusion and co-occurrence data with a minimum required interaction score of 0.4 and a maximum of 50 interactors in the first shell and 50 interactors in the second shell. Statistical significance of the enriched biological processes (GO BP categories) in the MT3 network was set with a false discovery rate (FDR) <0.05.

Identification of differentially expressed genes in resting WT compared to resting *Mt3^{-/-}* M ϕ was based on our previously published RNA-seq data (NCBI SRA: PRJNA533616) (19). The number of biological replicates used in the analysis was 3 per group. Genes differentially expressed with a fold change FC>2 and adjusted p value $q < 0.05$ were considered significant. The Benjamini-Hochberg correction was used to adjust p values for multiple hypothesis testing. Differentially expressed genes in *Mt3^{-/-}* BMDM ϕ compared to WT BMDM ϕ with $q < 0.05$ were queried using the functional annotation clustering tool DAVID to identify statistically enriched GO categories (using the GO terms, BP direct, CC direct and MF direct) in *Mt3^{-/-}* BMDM ϕ compared to WT BMDM ϕ (41). Significance of enrichment was set to FDR <0.05.

Gene Silencing

For gene silencing, M ϕ were transfected with the transfection complex (50 μ l) of siRNA and TransIT-TKO[®] (0.5%) transfection reagent (Mirus Bio[™]) in 500 μ l of complete RPMI 1640 medium without antibiotics as per the manufacturer's instructions. Concentration of siRNAs used for gene silencing were 100 nM each of the non-targeting pool (ON-TARGETplus[™] scramble siRNA), human *MT3* (MT3 Silencer[®] Pre-designed siRNA) and mouse *Ticam1* (ON-TARGETplus SMARTpool). All siRNAs were purchased from Dharmacon (GE Healthcare). Both BMDM ϕ and hM ϕ were incubated with the siRNA containing transfection complexes for 24h in RPMI medium and washed prior to transfection with LPS in Opti-MEM medium. TRIF silencing was assessed by protein expression using Western blots. Human *MT3* silencing was assessed by gene expression using qRT-PCR.

IFNAR1 Neutralization

IFNAR1 on WT and *Mt3^{-/-}* BMDM ϕ was neutralized using 10 μ g/ml monoclonal anti-IFNAR1 antibody (BioLegend; Clone: MAR1-5A3) 1h prior and 24h after iLPS (10 μ g/ml) stimulation. Negative control groups were treated with the same dose of isotype control IgG antibody (BioLegend; Clone: MOPC-21). After a total 48h, cell lysates and supernatants were harvested for the molecular analysis.

Non-Canonical Inflammasome Activation in M ϕ

To activate the non-canonical inflammasome, 1×10^6 M ϕ were transfected with a transfection complex (50 μ l) of 0.3% TransIT[™]-LT1 (Mirus Bio[™]) transfection reagent (vehicle) and 2 μ g/ml or 10 μ g/ml ultrapure LPS-B5 (*In vivo* Gen)

prepared from *E. coli* 055:K59(B5) in 500 μ l Opti-MEM medium (Thermo Fisher Scientific-US) as per manufacturer's instructions for 24h.

Preparation of Zn²⁺-Sufficient and Zn²⁺-Deficient Opti-MEM Media

Molecular biology grade chelex-100 resin (BioRad) was washed three times with metal free ddiH₂O prior to use. To prepare Zn²⁺-deficient Opti-MEM medium, washed Chelex-100 resin (3 g per 100 ml) was added to Opti-MEM media and vigorously shaken for 1h on an orbital shaker at room temperature. After this time, media was filtered using a 0.22 μ m filter and mixed with fresh washed chelex-100 resin and the same procedure was repeated for a total of 3 times to eliminate metals from Opti-MEM media. Chelex was removed from the media by a final filtration step. During each of these stages, an aliquot of the media was saved to monitor the efficiency of Ca²⁺, Mg²⁺, Mn²⁺, Co²⁺, Zn²⁺, Cu²⁺, Ni²⁺ and Fe²⁺ elimination by ICP-MS. The amount of Zn²⁺ in Opti-MEM media was decreased by 95% by the above chelation method. To prepare Zn²⁺-sufficient media, chelexed Opti-MEM was reconstituted with Ca²⁺, Mg²⁺, Mn²⁺, Co²⁺, Cu²⁺ and Zn²⁺ at the original concentrations as measured by ICP-MS. To prepare Zn²⁺-deficient media, all measured elements except Zn²⁺ were added to the chelexed Opti-MEM media at the original measured concentrations. Finally, the pH of Zn²⁺-sufficient and Zn²⁺-deficient Opti-MEM media was adjusted to 7.4 and filtered prior to use.

MT3 Overexpression and Purification

The pCMV6-Ac-GFP vector containing the mouse *Mt3* gene (pCMV6-Ac-MT3-GFP) and empty pCMV6-Ac-GFP vectors were acquired from Origene and dissolved in nuclease-free sterile H₂O. Plasmid DNA (5 ng) was added to 50 μ l of thawed Novablue competent *E. coli* cells (EMD Millipore) and transformation was performed as per manufacturer's instructions. *E. coli* cells were serially diluted in S. O. C media (ThermoFisher Scientific) and plated onto Luria-Bertani (LB) plates with 50 μ g/ml carbenicillin and grown for 24h at 37°C. A single colony was isolated and inoculated in LB media containing carbenicillin and grown at 37°C for 5h in a shaker. The culture was further amplified by passaging for another 24h. *E. coli* cells were then harvested by centrifugation at 2000 rpm for 10 mins. and plasmid was extracted using the EndoFree plasmid MAXI kit (Qiagen) as per the manufacturer's instructions. The plasmid was reconstituted in endotoxin-free TE buffer and OD readings obtained were in the range of 1.8-1.9. The resulting endotoxin-free plasmid DNA was set to a concentration of 1 mg/ml in filter-sterilized EndoFree TE buffer and frozen into aliquots until further use.

Mt1^{-/-}Mt2^{-/-} BMDM ϕ were transfected with pCMV6-Ac-GFP control vector or pCMV6-Ac-MT3-GFP vector using the LT1 transfection reagent (Mirus Bio) in RPMI media containing 10% serum without antibiotics as per the manufacturer's instructions. After 48h, BMDM ϕ cultures were lysed with 250 μ l of 0.1% SDS prepared in double-deionized (ddi) H₂O for 20 min. on ice with intermittent mixing. Cell lysates were transferred to 0.22 μ m

filter tubes and centrifuged at 13000 rpm for 5 mins. Filtered cell lysates were subjected to SEC-ICP-MS to isolate the MT3 protein as described below.

Preparation of apo-MT3, 4Zn²⁺-MT3 or 6Zn²⁺-MT3

Cell lysates from above were analyzed by SEC-ICP-MS to detect the MT3-associated peak, followed by collection of the fraction of interest (18-21 mins.). The collected fraction was concentrated by freeze drying in Millrock lyophilizer (Millrock, NY). The concentrated fraction was treated with 1 g of Chelex X-100 resin to remove the divalent metals associated to the protein. The total MT concentration was calculated by the total sulfur concentration in the sample with a 1:20 stoichiometry. The sample was divided into 3 fractions, and each fraction was incubated for 2 h in 50 mM Tris-HCl with the appropriate concentration of ⁶⁶Zn²⁺ nitrate to obtain an MT3-Zn²⁺ saturation of 0, 4 or 6 Zn²⁺ ions per MT3 molecule. After incubation, samples were filtered using a 3 kDa MWCO filter to remove the unbound Zn²⁺ and reconstituted in 1X PBS.

Transfection of Apo, Zn²⁺-MT3 Complexes Into BMDMφ

In a 24 well plate, 5 X 10⁵ *Mt3*^{-/-} BMDMφ were transfected with the transfection complex (10 μl) containing 500 ng of apo-MT3, 4Zn²⁺-MT3 or 6Zn²⁺-MT3 and Pro-JectTM (1.75 μl) protein transfection reagent (ThermoScientific-US) in 250 μl of 2% FBS containing antibiotic free RPMI 1640 medium. Control *Mt3*^{-/-} BMDMφ were treated with Pro-JectTM alone. Cells were incubated with the transfection complexes for 3.5h and washed two times using HBSS prior to challenge with iLPS in Zn²⁺ free Opti-MEM medium. At the experiment end point, cell lysates were either prepared for SEC-ICP-MS analysis or both cell lysates and supernatants were collected for the analysis of non-canonical inflammasome activation.

SEC-ICP-MS-MS Analysis and Normalization of Data

SEC-ICP-MS-MS analysis of WT and *Mt3*^{-/-} BMDMφ was performed as described previously (11). Mφ were plated in Opti-MEM media, and either left untreated or transfected with 10 μg/ml LPS for 1, 24 and 48h. After this time, Mφ were washed twice in HBSS and cells were lysed with 0.1% SDS on ice for 20 mins. Cell lysates were then centrifuged in 0.22 mm filter tubes at 13000 rpm for 10 mins. Filtered cell lysates were frozen at -80°C until further analysis by SEC-ICP-MS. 50-80 μl of cell lysates were injected to the HPLC-ICP-MS system according to protein concentration. To normalize the response of ICP-MS-MS signal from SEC separations on different days, 50 μl of 0.5 mg/ml carbonic anhydrase was injected into the liquid chromatography system, and area of Zn²⁺ signals from samples was normalized to area of the carbonic anhydrase peak from each day. The absorbance of carbonic anhydrase at 280 nm was followed to ensure protein integrity.

The instrumentation consisted of an Agilent 1100 HPLC equipped with a degasser, a binary pump, a thermostated auto sampler, a column oven compartment and a diode array

detector. For the Mφ lysates, a TSK gel 3000SW gel filtration column (TSK Tokyo Japan) 7.8 × 300 mm, 10 mm particle size was used. The mobile phase was ammonium acetate pH 7.4, 0.05% MeOH at 0.5 ml/minute. The HPLC system was coupled to the ICP-MS-MS nebulizer *via* a short polyether ether ketone capillary of 0.17 mm internal diameter. An Agilent 7500ce ICP-MS system equipped with a micromist quartz nebulizer, a chilled double pass Scott spray chamber and a standard 2 mm insert quartz torch with shield torch was used for all experiments. The ICP-MS was operated by the Agilent Mass Hunter integrated chromatographic software in the helium collision mode as reported previously (11). The isotope dilution experiments were processed by exporting the chromatographic data to Origin (Origin labs, CA) and the signal, in the form of counts per second, was used to calculate the ratio of ⁶⁶Zn²⁺/⁶⁴Zn²⁺ at every point in the chromatograms. This was used to generate a new chromatogram that reflected the input of ⁶⁶Zn²⁺ from the MT3-Zn²⁺ complex at every molecular mass region in the chromatogram. The total area under the chromatograms was used to calculate the concentration of total Zn²⁺ (⁶⁴Zn²⁺) and ⁶⁶Zn²⁺ from the MT3-⁶⁶Zn²⁺ complexes (⁶⁶Zn²⁺/⁶⁴Zn²⁺) against a calibration curve of Zn²⁺ based on carbonic anhydrase.

ICP-MS-MS and SEC-ICP-MS-MS Quality Control to Avoid External Zn²⁺ Contamination

All metal analysis experiments were performed using trace metal grade reagents with acid washed plastic vials. Reagent blanks were used to correct the background signal. The analysis was performed through a metal free encased auto sampler. The concentration of Zn²⁺ in the blanks was always below 100 parts per trillion (ppt), the blank estimate concentration on the calibration curves was always below 50 ppt, while the detection limits were below 30 ppt.

For chromatographic analysis, the mobile phase was cleaned using a Chelex 100 resin, using the batch method. In brief, 3 g of Chelex-100 was added to a liter of mobile phase, stirred for 30 mins. and passed through a 0.45 mm membrane. This decreased the Zn²⁺ concentration below 200 ppt (measured as total). By this method, the base line ICP-MS-MS ⁶⁶Zn²⁺ signal was below 1000 counts per second, which represents sub-ppb levels. The SEC column was cleaned using 10 volumes of 0.2 M NaCl and equilibrated with the mobile phase, followed by injection of 50 μl of 2% HNO₃ three times to remove any accumulated Zn²⁺ in the column. With this procedure, Zn²⁺ distribution in the samples never deviated more than 10% compared to the theoretical natural Zn²⁺ isotope distribution in the control Mφ samples. Four blanks and four carbonic anhydrase standards were injected after the cleaning procedure for monitoring Zn²⁺ signal by ICP-MS-MS to ensure optimal column performance. Typically, the column was cleaned every 30-40 samples.

LPS Treatment *In Vivo*

Thirteen-week-old WT and *Mt3*^{-/-} mice were primed with *i.p.* injection of 10 mg/kg poly(I:C) for 6h followed by 2 mg/kg ultrapure LPS-B5 (*In vivo*Gen) prepared from *E. coli* 055:K59 (B5) (*i.p.* injection) for 18h. At the experiment end point, blood

was collected by cardiac puncture, allowed to clot, and centrifuged at 2000 rpm for 30 mins. at 4°C to isolate serum. Serum was used to measure cytokines by enzyme-linked immunosorbent assay (ELISA).

In Vitro and In Vivo Infection With Gram-Negative Bacteria

For *in vitro* infection, *E. coli* (K12) was grown in LB broth at 37°C overnight in an orbital shaker. The culture was pelleted, washed and resuspended with ice-cold DPBS. Optical Density (OD) of the culture was measured at 600nm using a spectrophotometer. To analyze *E. coli* burden in *in vitro*, hM ϕ were transfected with scramble siRNA or *MT3* siRNA as described above. hM ϕ , WT and *Mt3*^{-/-} BMDM ϕ were infected with a multiplicity of infection (MOI) of 25 *E. coli*: 1 hM ϕ for 3.5h in Opti-MEM media. M ϕ were washed 3 times with 10 μ g/ml gentamycin sulfate containing DPBS to kill extracellular bacteria and incubated in Opti-MEM media with antibiotic for 24h. M ϕ were again washed 3 times with antibiotic-free DPBS, diH₂O was added and cells were incubated for 30 min. to induce osmotic lysis. Cells were scraped and lysates were diluted in DPBS followed by plating on LB agar plates and incubated at 37°C for 24h. Colonies were enumerated as above. Intracellular bacterial burden was represented as percent inhibition of bacterial growth in *MT3*-silenced hM ϕ compared to scramble siRNA treated hM ϕ and in *Mt3*^{-/-} BMDM ϕ compared to WT BMDM ϕ .

To analyze antibacterial immunity *in vivo*, 10 to 12 week-old mice were used. Mice were infected with *E. coli* 1 X 10⁹ CFUs *via i.p.* injection (300 μ l/mouse) for 1h or 6h. To investigate the role of NLRP3 inflammasome in antibacterial immunity, mice were treated with 1 mg/mouse MCC950 (an inhibitor of NLRP3 inflammasome) *via i.p.* injection (100 μ l/mouse) for 1h followed by *E. coli* 1 X 10⁹ CFUs *via i.p.* injection (300 μ l/mouse) for 6h. *K. pneumoniae* KP2 2-70, a virulent, heavily encapsulated gram-negative bacterial strain (89, 90), was grown overnight in brain heart infusion (BHI) broth. The following morning bacteria were washed with DPBS, and administered at 4 x 10⁴ CFUs in 50 μ l per mouse by the *i.n.* to isoflurane-anesthetized mice for 48h. At the infection end point, blood was collected by cardiac puncture. A portion of the blood sample was acquired in anticoagulant (3% Na-citrate or EDTA) containing tubes to determine bacterial CFUs in blood. The remaining blood was allowed to clot, and centrifuged at 2000 rpm for 30 mins. at 4°C to isolate serum. Peritoneal lavage was collected using ice-cold 10 ml DPBS. Kidney, lung, and spleen were collected after perfusion with 3 ml of DPBS, indicated organs and skin was rinsed in DPBS and ground with 5 ml DPBS using a glass grinder. Bacterial growth was measured in blood, peritoneal lavage, kidney, lung, skin and spleen samples. Serum and peritoneal lavage were used to measure cytokines by enzyme-linked immunosorbent assay (ELISA).

LPS-Induced Septic Shock

Septic shock was induced in mice *via i.p.* injection with ultrapure LPS-B5 (20 mg/kg) (*In vivo*Gen) prepared from *E. coli* 055:K59 (B5). Mice were weighed and sepsis scores were determined at

various intervals. The MSS scoring method assesses sepsis severity with scores ranging from 1-4 based on 7 parameters (appearance, consciousness, activity, stimulus (sounds/touch), eyes aspect, respiration rate and respiration quality) (27). Survival analysis was conducted using the Kaplan-Meier analysis method and log-rank (Mantel-Cox test) was used to determine statistical differences in survival.

In Vivo Infection With Gram-Positive Bacteria

A representative MIT1 clonal Group-A-Streptococcus GAS5448 was used for subcutaneous infections (91). GAS was grown at 37°C under static conditions in Todd-Hewitt broth (BD, MD, USA) supplemented with 1.5% yeast extract (BD Biosciences, MD, USA) and *in vivo* infections were performed as described previously (29, 92). WT and *Mt3*^{-/-} mice (n=8/group) were used in this study as a model for subcutaneous GAS infections. One day prior to infection, the hair on the back of the mice was depilated (using Nair cream) and mice were infected subcutaneously with 0.1 ml of GAS suspension prepared in sterile DPBS (Ca²⁺/Mg²⁺ free, low endotoxin, Mediatech, VA, USA, DPBS) (OD₆₀₀ adjusted to yield ~1-5x10⁸ (8) CFUs). Actual inoculum was determined by plating on trypticase soy agar containing 5% sheep blood (BD Biosciences, MD, USA). Mice were monitored twice daily for body weight, lesions, and mortality. To determine GAS dissemination and load, mice were humanely euthanized 72h post-infection. Blood was drawn through cardiac puncture; necrotic skin, kidney, and spleen were recovered aseptically and weighed. One ml of DPBS was added per 100 mg tissue and homogenized (Omni International, Marietta, GA) followed by plating of ten-fold dilutions on blood agar plates. GAS burden was calculated as colony-forming units (CFUs) per ml (blood) or per mg of tissue. The remaining homogenates were centrifuged for 15 mins. at 12,000 x g at 4°C, and supernatants were stored at -80°C for western blot analysis.

Gene Expression

RNA was isolated from M ϕ after elimination of genomic DNA using RNeasy Plus Mini kit (Qiagen) or QUICK-RNA™ MINIPREP KIT (Thomas Scientific). cDNA was prepared using Reverse Transcription Systems Kit (Promega, WI) or rAmp First Strand cDNA Synthesis Flex Kit (Thomas Scientific). Taqman primer/probe sets (Applied Biosystems, CA) were used for real-time gene expression analysis using ABI Prism 7500. For time course analysis of expression of murine *Mt* genes, M ϕ were left unstimulated or stimulated with 2 μ g/ml iLPS for 0h, 1h, 6h, 24h and 48h. Data are presented as fold change in gene expression normalized to unstimulated M ϕ at the 0h time point. To examine the effects of extracellular ultrapure LPS (exLPS) on murine *Mt3* gene expression, BMDM ϕ were left unstimulated or stimulated with 10 μ g/ml exLPS. Data are presented as fold change in gene expression normalized to unstimulated M ϕ at the 48h time point. For *MT2A* gene expression analysis in *MT3* silenced hM ϕ , cells were treated with either *MT3* siRNA or scramble siRNA as mentioned above. Data are presented as fold change in gene expression normalized to control siRNA treated hM ϕ .

Hypoxanthine guanine phosphoribosyl transferase (*Hprt*) was used as an internal control to compare target gene expression.

Western Blotting

TRIF (Proteintech), pIRF3 (BIOSS), STAT1, pSTAT1 (Abcam), GBP2, GBP5 (Proteintech), caspase-11 (Abcam and eBioscience™), CASPASE-4 (MBL), Gasdermin D (Proteintech and Cell Signaling Technologies), caspase-1 (AdipoGen Life Sciences), IL-1 β (R&D Systems) and caspase-8 (Enzo Life Sciences) were assessed in kidney homogenates of *E. coli* infected mice. Cell lysates were prepared using Denaturing Cell Extraction Buffer (Invitrogen) containing protease & phosphatase inhibitor cocktail (ThermoScientific). Culture supernatants were frozen at -80°C until use and processed using methanol-chloroform protein extraction method. Briefly, supernatants were mixed with equal volume of 100% ice-cold methanol and 0.25 times of the total volume of chloroform followed by gentle vortexing and centrifugation at 20,000 X g at 4°C for 10 min. Upper-phase was discarded without disturbing inter-phase proteins. Ice-cold methanol (500 μ l) was added to the tube, gently vortexed and centrifuged at 20,000 X g at 4°C for 10 mins. Supernatants were discarded and pellet was dried at 37°C for 3-5 mins. Urea (8 M, pH-8.0) was used to dissolve the pellet and extracted proteins were stored at -80°C. Total cell lysates, supernatants proteins, cell lysates + supernatants and kidney homogenates were boiled in SDS-PAGE 1X sample buffer at 95°C for 5 mins. Kidney homogenates were centrifuged at 20,000 X g at 4°C for 15 mins. Supernatants were collected for protein analysis. Reduced proteins were run on 8%,10% or 12% SDS-PAGE gels and transferred on to 0.22 μ m nitrocellulose membranes (GE Healthcare Life Sciences). Membranes were blocked using 5% skim milk in 1X Tris-buffered saline and 0.1% Tween 20 (1XTBST) and probed overnight with primary antibodies at 4°C. Membranes were washed 3 times for 10 mins. each with 1XTBST and probed with corresponding HRP conjugated or IRDyes (LI-COR) secondary antibodies, washed and developed using BrightStar™ Femto HRP Chemiluminescent 2-Component Substrate Kit (Alkali Scientific Inc. β -actin was used as an internal loading control. Western blots were analyzed using ImageJ software and densitometry data were normalized to β -actin.

ELISA

Human and mouse IL-1 β (BioLegend) concentration in media supernatants, serum and in peritoneal lavage and mouse IL-1 α (BioLegend) in media supernatants were determined using commercial ELISA kits according to the manufacturer's instructions.

Quantification and Statistical Analysis

Data were analyzed using Sigma plot or GraphPad Prism by one-way ANOVA for multiple comparisons using the indicated *ad-hoc* methods with at least 3 or more independent biological replicates. Where two groups were compared, two-tailed t-test was used. For *in vivo* infection, bacterial CFUs were log-transformed for statistical analysis. p values were calculated, *p < 0.05, **p < 0.01, ***p < 0.001; NS, not significant, ND, not detected.

DATA AVAILABILITY STATEMENT

The original contributions presented in the study are included in the article/**Supplementary Material**, further inquiries can be directed to the corresponding author.

ETHICS STATEMENT

All animal studies were reviewed and approved by the Institutional Animal Care and Use Committee (IACUC) at the University of Cincinnati and were conducted within the Department of Laboratory Animal Medicine accredited by American Association for Accreditation of Laboratory Animal Care (Frederick, MD). All animal experiments were conducted in accordance with Animal Welfare Act guidelines of the National Institutes of Health.

AUTHOR CONTRIBUTIONS

DC and KSV planned and conducted molecular and biochemical *in vitro* and *in vivo* experiments, generated *Casp-11^{-/-}Mt3^{-/-}* and *Lys2Cre Mt3^{fl/fl}* mice, analyzed data, and wrote the manuscript. JG conducted *in vivo* infections with *K. pneumoniae*. AS, SN, and SM conducted *in vivo* experiments with GAS infection and analyzed data. AP assisted with bioinformatics analysis. JL conducted chromatographic and mass spectrometric analysis using ICP-MS and SEC-ICP-MS and MT3-Zn²⁺ complex preparations, and analyzed data. KSV designed and supervised the project. All authors contributed to the article and approved the submitted version.

FUNDING

This work was supported by a Junior Faculty Pilot Project Award, American Heart Association 19CDA34770022 Award, American Association of Immunology Careers in Immunology Fellowship Awards to KSV and NIAIDR01 AI106269-06 awarded in part to KSV. GAS studies were supported by the UND CoBRE Host-Pathogen Interactions Pilot Award - NIH/NIGMS award P20GM113123, UND SMHS funds (SN), and UND VPRED Postdoctoral funding support (AS).

ACKNOWLEDGMENTS

We thank Transgenic Animal and Genome Editing Core at Cincinnati Children's Hospital Medical (CCHMC) Center for production of *Mt3^{fl/fl}* mice.

SUPPLEMENTARY MATERIAL

The Supplementary Material for this article can be found online at: <https://www.frontiersin.org/articles/10.3389/fimmu.2021.755961/full#supplementary-material>

REFERENCES

- Haque M, Sartelli M, McKimm J, Abu Bakar M. Health Care-Associated Infections - an Overview. *Infect Drug Resist* (2018) 11:2321–33. doi: 10.2147/IDR.S177247
- Kayagaki N, Kagawa S, Hamada H, Ariyoshi T. Non-Canonical Inflammasome Activation Targets Caspase-11. *Nature* (2011) 479:117–21. doi: 10.1038/nature10558
- Vanaja SK, Russo AJ, Behl B, Banerjee I, Yankova M, Deshmukh SD, et al. Bacterial Outer Membrane Vesicles Mediate Cytosolic Localization of LPS and Caspase-11 Activation. *Cell* (2016) 165:1106–19. doi: 10.1016/j.cell.2016.04.015
- Liu X, Zhang Z, Ruan J, Pan Y, Magupalli VG, Wu H, et al. Inflammasome-Activated Gasdermin D Causes Pyroptosis by Forming Membrane Pores. *Nature* (2016) 535:153–8. doi: 10.1038/nature18629
- Davis SR, Cousins RJ. Metallothionein Expression in Animals: A Physiological Perspective on Function. *J Nutr* (2000) 130:1085–8. doi: 10.1093/jn/130.5.1085
- Kimura T, Kambe T. The Functions of Metallothionein and ZIP and ZnT Transporters: An Overview and Perspective. *Int J Mol Sci* (2016) 17:336. doi: 10.3390/ijms17030336
- Krezel A, Maret W. The Functions of Metamorphic Metallothioneins in Zinc and Copper Metabolism. *Int J Mol Sci* (2017) 18:1237. doi: 10.3390/ijms18061237
- Palmeter RD. The Elusive Function of Metallothioneins. *Proc Natl Acad Sci U S A* (1998) 95:8428–30. doi: 10.1073/pnas.95.15.8428
- Subramanian Vignesh K, Landero Figueroa JA, Porollo A, Caruso JA, Deepe GS Jr. Granulocyte Macrophage-Colony Stimulating Factor Induced Zn Sequestration Enhances Macrophage Superoxide and Limits Intracellular Pathogen Survival. *Immunity* (2013) 39:697–710. doi: 10.1016/j.immuni.2013.09.006
- Wu A, Tymoszuk P, Haschka D, Heeke S, Dichtl S, Petzer V, et al. Salmonella Utilizes Zinc To Subvert Antimicrobial Host Defense of Macrophages via Modulation of NF-kappaB Signaling. *Infect Immun* (2017) 85:e00418–17. doi: 10.1128/IAI.00418-17
- Subramanian Vignesh K, Landero Figueroa JA, Porollo A, Divanovic S, Caruso JA, Deepe GS Jr. IL-4 Induces Metallothionein 3- and SLC30A4-Dependent Increase in Intracellular Zn(2+) That Promotes Pathogen Persistence in Macrophages. *Cell Rep* (2016) 16:3232–46. doi: 10.1016/j.celrep.2016.08.057
- Shankar AH, Prasad AS. Zinc and Immune Function: The Biological Basis of Altered Resistance to Infection. *Am J Clin Nutr* (1998) 68:447S–63S. doi: 10.1093/ajcn/68.2.447S
- Pyle CJ, Akhter S, Bao S, Dodd CE, Schlesinger LS, Knoell DL. Zinc Modulates Endotoxin-Induced Human Macrophage Inflammation Through ZIP8 Induction and C/EBPbeta Inhibition. *PLoS One* (2017) 12:e0169531. doi: 10.1371/journal.pone.0169531
- Haase H, Ober-Blöbaum JL, Engelhardt G, Hebel S, Heit A, Heine H, et al. Zinc Signals are Essential for Lipopolysaccharide-Induced Signal Transduction in Monocytes. *J Immunol* (2008) 181:6491–502. doi: 10.4049/jimmunol.181.9.6491
- von Bulow V, Rink L, Haase H. Zinc-Mediated Inhibition of Cyclic Nucleotide Phosphodiesterase Activity and Expression Suppresses TNF-Alpha and IL-1 Beta Production in Monocytes by Elevation of Guanosine 3',5'-Cyclic Monophosphate. *J Immunol* (2005) 175:4697–705. doi: 10.4049/jimmunol.175.7.4697
- Gong T, Yang Y, Jin T, Jiang W, Zhou R. Orchestration of NLRP3 Inflammasome Activation by Ion Fluxes. *Trends Immunol* (2018) 39:393–406. doi: 10.1016/j.it.2018.01.009
- Summersgill H, England H, Lopez-Castejon G, Lawrence CB, Luheshi NM, Pahle J, et al. Zinc Depletion Regulates the Processing and Secretion of IL-1beta. *Cell Death Dis* (2014) 5:e1040. doi: 10.1038/cddis.2013.547
- Brough D, Pelegrin P, Rothwell NJ. Pannexin-1-Dependent Caspase-1 Activation and Secretion of IL-1beta is Regulated by Zinc. *Eur J Immunol* (2009) 39:352–8. doi: 10.1002/eji.200838843
- Chowdhury D, Alrfai H, Landero Figueroa JA, Candor K, Porollo A, Fecher R, et al. Metallothionein 3 Controls the Phenotype and Metabolic Programming of Alternatively Activated Macrophages. *Cell Rep* (2019) 27:3873–86.e3877. doi: 10.1016/j.celrep.2019.05.093
- Rathinam VA, Vanaja SK, Waggoner L, Sokolovska A, Becker C, Stuart LM, et al. TRIF Licenses Caspase-11-Dependent NLRP3 Inflammasome Activation by Gram-Negative Bacteria. *Cell* (2012) 150:606–19. doi: 10.1016/j.cell.2012.07.007
- Lee SJ, Koh JY. Roles of Zinc and Metallothionein-3 in Oxidative Stress-Induced Lysosomal Dysfunction, Cell Death, and Autophagy in Neurons and Astrocytes. *Mol Brain* (2010) 3:30. doi: 10.1186/1756-6606-3-30
- Szklarczyk D, Gable AL, Lyon D, Junge A, Wyder S, Huerta-Cepas J, et al. STRING V11: Protein-Protein Association Networks With Increased Coverage, Supporting Functional Discovery in Genome-Wide Experimental Datasets. *Nucleic Acids Res* (2019) 47:D607–13. doi: 10.1093/nar/gky1131
- Kim B, Lee Y, Kim E, Kwak A, Ryoo S, Bae SH, et al. The Interleukin-1alpha Precursor is Biologically Active and is Likely a Key Alarmin in the IL-1 Family of Cytokines. *Front Immunol* (2013) 4:391. doi: 10.3389/fimmu.2013.00391
- Kurt-Jones EA, Beller DI, Mizel SB, Unanue ER. Identification of a Membrane-Associated Interleukin 1 in Macrophages. *Proc Natl Acad Sci U S A* (1985) 82:1204–8. doi: 10.1073/pnas.82.4.1204
- Fettelschoss A, Kistowska M, LeibundGut-Landmann S, Beer HD, Johansen P, Senti G, et al. Inflammasome Activation and IL-1beta Target IL-1alpha for Secretion as Opposed to Surface Expression. *Proc Natl Acad Sci U S A* (2011) 108:18055–60. doi: 10.1073/pnas.1109176108
- Casson CN, Yu J, Reyes VM, Taschuk FO, Yadav A, Copenhaver AM, et al. Human Caspase-4 Mediates Noncanonical Inflammasome Activation Against Gram-Negative Bacterial Pathogens. *Proc Natl Acad Sci U S A* (2015) 112:6688–93. doi: 10.1073/pnas.1421699112
- Shrum B, Anantha RV, Xu SX, Donnelly M, Haeryfar SM, McCormick JK, et al. A Robust Scoring System to Evaluate Sepsis Severity in an Animal Model. *BMC Res Notes* (2014) 7:1–11. doi: 10.1186/1756-0500-7-233
- Hara H, Seregin SS, Yang D, Fukase K, Chamailard M, Alnemri ES, et al. The NLRP6 Inflammasome Recognizes Lipoteichoic Acid and Regulates Gram-Positive Pathogen Infection. *Cell* (2018) 175:1651–1664 e1614. doi: 10.1016/j.cell.2018.09.047
- Chella Krishnan K, Mukundan S, Alagarsamy J, Hur J, Nookala S, Siemens N, et al. Genetic Architecture of Group A Streptococcal Necrotizing Soft Tissue Infections in the Mouse. *PLoS Pathog* (2016) 12:e1005732. doi: 10.1371/journal.ppat.1005732
- Wang J, Shao Y, Wang W, Li S, Xin N, Xie F, et al. Caspase-11 Deficiency Impairs Neutrophil Recruitment and Bacterial Clearance in the Early Stage of Pulmonary Klebsiella Pneumoniae Infection. *Int J Med Microbiol* (2017) 307:490–6. doi: 10.1016/j.ijmm.2017.09.012
- Aachoui Y, Leaf IA, Hagar JA, Fontana MF, Campos CG, Zak DE, et al. Caspase-11 Protects Against Bacteria That Escape the Vacuole. *Science* (2013) 339:975–8. doi: 10.1126/science.1230751
- Broz P, Ruby T, Belhocine K, Bouley DM, Kayagaki N, Dixit VM, et al. Caspase-11 Increases Susceptibility to Salmonella Infection in the Absence of Caspase-1. *Nature* (2012) 490:288–91. doi: 10.1038/nature11419
- Krause K, Daily K, Estfanous S, Hamilton K, Badr A, Abu Khweek A, et al. Caspase-11 Counteracts Mitochondrial ROS-Mediated Clearance of Staphylococcus Aureus in Macrophages. *EMBO Rep* (2019) 20:e48109. doi: 10.15252/embr.201948109
- Kovacs SB, Oh C, Maltez VI, McLaughlin BD, Verma A, Miao EA, et al. Neutrophil Caspase-11 Is Essential to Defend Against a Cytosol-Invasive Bacterium. *Cell Rep* (2020) 32:107967. doi: 10.1016/j.celrep.2020.107967
- Cerqueira DM, Gomes MTR, Silva ALN, Rungue M, Assis NRG, Guimarães ES, et al. Guanylate-Binding Protein 5 Licenses Caspase-11 for Gasdermin-D Mediated Host Resistance to Brucella Abortus Infection. *PLoS Pathog* (2018) 14:e1007519. doi: 10.1371/journal.ppat.1007519
- Wang K, Sun Q, Zhong X, Zeng M, Zeng H, Shi X, et al. Structural Mechanism for GSDMD Targeting by Autoprocessed Caspases in Pyroptosis. *Cell* (2020) 180:941–955 e920. doi: 10.1016/j.cell.2020.02.002
- Mandal P, Feng Y, Lyons JD, Berger SB, Otani S, DeLaney A, et al. Caspase-8 Collaborates With Caspase-11 to Drive Tissue Damage and Execution of Endotoxic Shock. *Immunity* (2018) 49:42–55 e46. doi: 10.1016/j.immuni.2018.06.011
- Antonopoulos C, Russo HM, El Sanadi C, Martin BN, Li X, Kaiser WJ, et al. Caspase-8 as an Effector and Regulator of NLRP3 Inflammasome Signaling. *J Biol Chem* (2015) 290:20167–84. doi: 10.1074/jbc.M115.652321

39. Santos JC, Dick MS, Lagrange B, Degrandi D, Pfeffer K, Yamamoto M, et al. LPS Targets Host Guanylate-Binding Proteins to the Bacterial Outer Membrane for non-Canonical Inflammasome Activation. *EMBO J* (2018) 37:e98089. doi: 10.15252/embj.201798089
40. Lagrange B, Benaoudia S, Wallet P, Magnotti F, Provost A, Michal F, et al. Human Caspase-4 Detects Tetra-Acylated LPS and Cytosolic Francisella and Functions Differently From Murine Caspase-11. *Nat Commun* (2018) 9:242. doi: 10.1038/s41467-017-02682-y
41. Huang da W, Sherman BT, Lempicki RA. Systematic and Integrative Analysis of Large Gene Lists Using DAVID Bioinformatics Resources. *Nat Protoc* (2009) 4:44–57. doi: 10.1038/nprot.2008.211
42. Durfee LA, Huibregtse JM. Identification and Validation of ISG15 Target Proteins. *Subcell Biochem* (2010) 54:228–37. doi: 10.1007/978-1-4419-6676-6_18
43. Pletneva LM, Haller O, Porter DD, Prince GA, Blanco JCG. Induction of Type I Interferons and Interferon-Inducible Mx Genes During Respiratory Syncytial Virus Infection and Reinfection in Cotton Rats. *J Gen Virol* (2008) 89:261–70. doi: 10.1099/vir.0.83294-0
44. Varela M, Diaz-Rosales P, Pereiro P, Forn-Cuní G, Costa MM, Dios S, et al. Interferon-Induced Genes of the Expanded IFIT Family Show Conserved Antiviral Activities in non-Mammalian Species. *PLoS One* (2014) 9:e100015. doi: 10.1371/journal.pone.0100015
45. Tirumurugan KG, Pawar RM, Dhinakar Raj G, Thangavelu A, Hammond JA, Parida S. RNAseq Reveals the Contribution of Interferon Stimulated Genes to the Increased Host Defense and Decreased PPR Viral Replication in Cattle. *Viruses* (2020) 12:463. doi: 10.3390/v12040463
46. Hojyo S, Fukada T. Roles of Zinc Signaling in the Immune System. *J Immunol Res* (2016) 2016:6762343. doi: 10.1155/2016/6762343
47. Maret W. Metals on the Move: Zinc Ions in Cellular Regulation and in the Coordination Dynamics of Zinc Proteins. *BioMetals* (2011) 24:411–8. doi: 10.1007/s10534-010-9406-1
48. Brieger A, Rink L, Haase H. Differential Regulation of TLR-Dependent MyD88 and TRIF Signaling Pathways by Free Zinc Ions. *J Immunol* (2013) 191:1808–17. doi: 10.4049/jimmunol.1301261
49. Zasloná Z, Flis E, Wilk MM, Carroll RG, Palsson-McDermott EM, Hughes MM, et al. Caspase-11 Promotes Allergic Airway Inflammation. *Nat Commun* (2020) 11:1055. doi: 10.1038/s41467-020-14945-2
50. Finethy R, Dockerman J, Kutsch M, Orench-Rivera N, Wallace GD, Piro AS, et al. Dynamin-Related Irgm Proteins Modulate LPS-Induced Caspase-11 Activation and Septic Shock. *EMBO Rep* (2020) 21:e50830. doi: 10.15252/embr.202050830
51. Chen R, Zeng L, Zhu S, Liu J, Zeh HJ, Kroemer G, et al. cAMP Metabolism Controls Caspase-11 Inflammasome Activation and Pyroptosis in Sepsis. *Sci Adv* (2019) 5:eav5562. doi: 10.1126/sciadv.aav5562
52. Chu LH, Indramohan M, Ratsimandresy RA, Gangopadhyay A, Morris EP, Monack DM, et al. The Oxidized Phospholipid oxPAPC Protects From Septic Shock by Targeting the non-Canonical Inflammasome in Macrophages. *Nat Commun* (2018) 9:996. doi: 10.1038/s41467-018-03409-3
53. Subramanian Vignesh K, Deepe GS Jr. Metallothioneins: Emerging Modulators in Immunity and Infection. *Int J Mol Sci* (2017) 18:2197. doi: 10.3390/ijms18102197
54. Dalton T, Palmiter RD, Andrews GK. Transcriptional Induction of the Mouse Metallothionein-I Gene in Hydrogen Peroxide-Treated Hepa Cells Involves a Composite Major Late Transcription Factor/Antioxidant Response Element and Metal Response Promoter Elements. *Nucleic Acids Res* (1994) 22:5016–23. doi: 10.1093/nar/22.23.5016
55. Chowdhury D, Deepe GS, Subramanian Vignesh K. The Metallothionein-Zinc Landscape: How It Shapes Antimicrobial Immunity. In: *Zinc Signaling*. Singapore: Springer (2019). p. 57–77.
56. Botella H, Peyron P, Levillain F, Poincloux R, Poquet Y, Brandli I, et al. Mycobacterial P(1)-Type ATPases Mediate Resistance to Zinc Poisoning in Human Macrophages. *Cell Host Microbe* (2011) 10:248–59. doi: 10.1016/j.chom.2011.08.006
57. Palmiter RD, Findley SD, Whitmore TE, Durnam DM. MT-III, a Brain-Specific Member of the Metallothionein Gene Family. *Proc Natl Acad Sci U S A* (1992) 89:6333–7. doi: 10.1073/pnas.89.14.6333
58. Leibbrandt ME, Koropatnick J. Activation of Human Monocytes With Lipopolysaccharide Induces Metallothionein Expression and is Diminished by Zinc. *Toxicol Appl Pharmacol* (1994) 124:72–81. doi: 10.1006/taap.1994.1010
59. Arizono K, Kagawa S, Hamada H, Ariyoshi T. Nitric Oxide Mediated Metallothionein Induction by Lipopolysaccharide. *Res Commun Mol Pathol Pharmacol* (1995) 90:49–58.
60. Coordinators NR. Database Resources of the National Center for Biotechnology Information. *Nucleic Acids Res* (2016) 44:D7–19. doi: 10.1093/nar/gkx1095
61. Stocks CJ, von Pein JB, Curson JEB, Rae J, Phan MD, Foo D, et al. Frontline Science: LPS-Inducible SLC30A1 Drives Human Macrophage-Mediated Zinc Toxicity Against Intracellular Escherichia Coli. *J Leukoc Biol* (2021) 109:287–97. doi: 10.1002/JLB.2HI0420-160R
62. Stocks CJ, Phan MD, Achard MES, Nhu NTK, Condon ND, Gawthorne JA, et al. Uropathogenic Escherichia Coli Employs Both Evasion and Resistance to Subvert Innate Immune-Mediated Zinc Toxicity for Dissemination. *Proc Natl Acad Sci U S A* (2019) 116:6341–50. doi: 10.1073/pnas.1820870116
63. Case CL, Kohler LJ, Lima JB, Strowig T, de Zoete MR, Flavell RA, et al. Caspase-11 Stimulates Rapid Flagellin-Independent Pyroptosis in Response to Legionella Pneumophila. *Proc Natl Acad Sci U S A* (2013) 110:1851–6. doi: 10.1073/pnas.1211521110
64. Akhter A, Caution K, Abu Khweek A, Tazi M, Abdulrahman BA, Abdelaziz DH, et al. Caspase-11 Promotes the Fusion of Phagosomes Harboring Pathogenic Bacteria With Lysosomes by Modulating Actin Polymerization. *Immunity* (2012) 37:35–47. doi: 10.1016/j.immuni.2012.05.001
65. Knodler LA, Crowley SM, Sham HP, Yang H, Wrande M, Ma C, et al. Noncanonical Inflammasome Activation of Caspase-4/Caspase-11 Mediates Epithelial Defenses Against Enteric Bacterial Pathogens. *Cell Host Microbe* (2014) 16:249–56. doi: 10.1016/j.chom.2014.07.002
66. Kobayashi T, Ogawa M, Sanada T, Mimuro H, Kim M, Ashida H, et al. The Shigella OspC3 Effector Inhibits Caspase-4, Antagonizes Inflammatory Cell Death, and Promotes Epithelial Infection. *Cell Host Microbe* (2013) 13:570–83. doi: 10.1016/j.chom.2013.04.012
67. Codo AC, Saraiva AC, Dos Santos LL, Visconde MF, Gales AC, Zamboni DS, et al. Inhibition of Inflammasome Activation by a Clinical Strain of Klebsiella Pneumoniae Impairs Efferocytosis and Leads to Bacterial Dissemination. *Cell Death Dis* (2018) 9:1182. doi: 10.1038/s41419-018-1214-5
68. Krause K, Caution K, Badr A, Hamilton K, Saleh A, Patel K, et al. CASP4/caspase-11 Promotes Autophagosome Formation in Response to Bacterial Infection. *Autophagy* (2018) 14:1928–42. doi: 10.1080/15548627.2018.1491494
69. Mueller NJ, Wilkinson RA, Fishman JA. Listeria Monocytogenes Infection in Caspase-11-Deficient Mice. *Infect Immun* (2002) 70:2657–64. doi: 10.1128/IAI.70.5.2657-2664.2002
70. LaRock CN, Nizet V. Inflammasome/IL-1beta Responses to Streptococcal Pathogens. *Front Immunol* (2015) 6:518. doi: 10.3389/fimmu.2015.00518
71. Hancz D, Westerlund E, Bastiat-Sempe B, Sharma O, Valfridsson C, Meyer L, et al. Inhibition of Inflammasome-Dependent Interleukin 1beta Production by Streptococcal NAD(+) Glycohydrolase: Evidence for Extracellular Activity. *mBio* (2017) 8:e00756–17. doi: 10.1128/mBio.00756-17
72. Valderrama JA, Riestra AM, Gao NJ, LaRock CN, Gupta N, Ali SR, et al. Group A Streptococcal M Protein Activates the NLRP3 Inflammasome. *Nat Microbiol* (2017) 2:1425–34. doi: 10.1038/s41564-017-0005-6
73. Reboldi A, Dang EV, McDonald JG, Liang G, Russell DW, Cyster JG. Inflammation. 25-Hydroxycholesterol Suppresses Interleukin-1-Driven Inflammation Downstream of Type I Interferon. *Science* (2014) 345:679–84. doi: 10.1126/science.1254790
74. Guarda G, Braun M, Staehli F, Tardivel A, Mattmann C, Förster I, et al. Type I Interferon Inhibits Interleukin-1 Production and Inflammasome Activation. *Immunity* (2011) 34:213–23. doi: 10.1016/j.immuni.2011.02.006
75. Sayadi A, Nguyen AT, Bard FA, Bard-Chapeau EA. Zip14 Expression Induced by Lipopolysaccharides in Macrophages Attenuates Inflammatory Response. *Inflamm Res* (2013) 62:133–43. doi: 10.1007/s00011-012-0559-y
76. Wessels I, Maywald M, Rink L. Zinc as a Gatekeeper of Immune Function. *Nutrients* (2017) 9:1286. doi: 10.3390/nu9121286
77. Maywald M, Wessels I, Rink L. Zinc Signals and Immunity. *Int J Mol Sci* (2017) 18:2222. doi: 10.3390/ijms18102222
78. Foster M, Samman S. Zinc and Regulation of Inflammatory Cytokines: Implications for Cardiometabolic Disease. *Nutrients* (2012) 4:676–94. doi: 10.3390/nu4070676
79. Prasad AS, Beck FW, Grabowski SM, Kaplan J, Mathog RH. Zinc Deficiency: Changes in Cytokine Production and T-Cell Subpopulations in Patients With

- Head and Neck Cancer and in Noncancer Subjects. *Proc Assoc Am Physicians* (1997) 109:68–77.
80. Beck FW, Li Y, Bao B, Prasad AS, Sarkar FH. Evidence for Reprogramming Global Gene Expression During Zinc Deficiency in the HUT-78 Cell Line. *Nutrition* (2006) 22:1045–56. doi: 10.1016/j.nut.2006.08.001
 81. Prasad AS. Zinc: Mechanisms of Host Defense. *J Nutr* (2007) 137:1345–9. doi: 10.1093/jn/137.5.1345
 82. Yuan CL, Hu YC. A Transgenic Core Facility's Experience in Genome Editing Revolution. *Adv Exp Med Biol* (2017) 1016:75–90. doi: 10.1007/978-3-319-63904-8_4
 83. Haeussler M, Schönig K, Eckert H, Eschstruth A, Mianné J, Renaud JB, et al. Evaluation of Off-Target and on-Target Scoring Algorithms and Integration Into the Guide RNA Selection Tool CRISPOR. *Genome Biol* (2016) 17:148. doi: 10.1186/s13059-016-1012-2
 84. Ran FA, Hsu PD, Wright J, Agarwala V, Scott DA, Zhang F. Genome Engineering Using the CRISPR-Cas9 System. *Nat Protoc* (2013) 8:2281–308. doi: 10.1038/nprot.2013.143
 85. Chen B, Gilbert LA, Cimini BA, Schnitzbauer J, Zhang W, Li GW, et al. Dynamic Imaging of Genomic Loci in Living Human Cells by an Optimized CRISPR/Cas System. *Cell* (2013) 155:1479–91. doi: 10.1016/j.cell.2013.12.001
 86. Valerius MT, Patterson LT, Witte DP, Potter SS. Microarray Analysis of Novel Cell Lines Representing Two Stages of Metanephric Mesenchyme Differentiation. *Mech Dev* (2002) 112:219–32. doi: 10.1016/S0925-4773(02)00008-4
 87. Wang H, Yang H, Shivalila CS, Dawlaty MM, Cheng AW, Zhang F, et al. One-Step Generation of Mice Carrying Mutations in Multiple Genes by CRISPR/Cas-Mediated Genome Engineering. *Cell* (2013) 153:910–8. doi: 10.1016/j.cell.2013.04.025
 88. Yang H, Wang H, Jaenisch R. Generating Genetically Modified Mice Using CRISPR/Cas-Mediated Genome Engineering. *Nat Protoc* (2014) 9:1956–68. doi: 10.1038/nprot.2014.134
 89. Domenico P, Diedrich DL, Straus DC. Extracellular Polysaccharide Production by *Klebsiella Pneumoniae* and its Relationship to Virulence. *Can J Microbiol* (1985) 31:472–8. doi: 10.1139/m85-088
 90. Wei RQ, Yee JB, Straus DC, Hutson JC. Bactericidal Activity of Testicular Macrophages. *Biol Reprod* (1988) 38:830–5. doi: 10.1095/biolreprod.38.4.830
 91. Chatellier S, Ihendyane N, Kansal RG, Khambaty F, Basma H, Norrby-Teglund A, et al. Genetic Relatedness and Superantigen Expression in Group A Streptococcus Serotype M1 Isolates From Patients With Severe and Nonsevere Invasive Diseases. *Infect Immun* (2000) 68:3523–34. doi: 10.1128/IAI.68.6.3523-3534.2000
 92. Nookala S, Mukundan S, Fife A, Alagarsamy J, Kotb M. Heterogeneity in FoxP3- and GARP/LAP-Expressing T Regulatory Cells in an HLA Class II Transgenic Murine Model of Necrotizing Soft Tissue Infections by Group A Streptococcus. *Infect Immun* (2018) 86:e00432–18. doi: 10.1128/IAI.00432-18

Conflict of Interest: The authors declare that the research was conducted in the absence of any commercial or financial relationships that could be construed as a potential conflict of interest.

Publisher's Note: All claims expressed in this article are solely those of the authors and do not necessarily represent those of their affiliated organizations, or those of the publisher, the editors and the reviewers. Any product that may be evaluated in this article, or claim that may be made by its manufacturer, is not guaranteed or endorsed by the publisher.

Copyright © 2021 Chowdhury, Gardner, Satpati, Nookala, Mukundan, Porollo, Landero Figueroa and Subramanian Vignesh. This is an open-access article distributed under the terms of the Creative Commons Attribution License (CC BY). The use, distribution or reproduction in other forums is permitted, provided the original author(s) and the copyright owner(s) are credited and that the original publication in this journal is cited, in accordance with accepted academic practice. No use, distribution or reproduction is permitted which does not comply with these terms.